A MATERIAL CHARACTERIZATION TECHNIQUE FOR DETECTION OF MICROCRACKS AND GRAIN STRUCTURES IN MINIATURIZED MICROELECTRIC DEVICES

Thesis

Submitted to

The School of Engineering of the

UNIVERSITY OF DAYTON

In Partial Fulfillment of the Requirement for

The Degree

Master of Science in Materials Engineering

By

Carl James Druffner

UNIVERSITY OF DAYTON

Dayton, Ohio

August 2002

A MATERIAL CHARACTERIZATION TECHNIQUE FOR DETECTION OF MICROCRACKS AND GRAIN STRUCTURES IN MINIATURIZED MICROELECTRIC DEVICES

APPROVED BY:

ABSTRACT

A MATERIAL CHARACTERIZATION TECHNIQUE FOR DETECTION OF MICROCRACKS AND GRAIN STRUCTURES IN MINIATURIZED MICROELECTRIC DEVICES

Druffner, Carl James
University of Dayton 2002

Advisor: Dr. S. Sathish

A material characterization technique has been developed for the investigation, detection and study of microcracks and the analysis of grain structures in microelectronic devices. As electronic devices are miniaturized the bulk mechanical material properties may begin to deviate from those calculated on a large scale material test to the small scale device. A characterization method that posses both high resolution and detection capabilities is necessary to ensure that minimizing the component does not in turn effect the operational ability or the manufacturing specifications or design tolerances for the device. While the majority of material characteristics of microelectronic devices are measured through electrical and magnetic properties, this technique utilizes elastic properties.

The Atomic Force Microscope (AFM) is routinely used for the surface characterization of nano structured materials. The Ultrasonic Force Microscope (UFM) uses the probe tip of the AFM to detect an ultrasonic wave that is being propagated through the sample material. The combination of AFM-UFM allows a near field acoustic microscopic image to be generated that produces a better characterization of the changes effecting the material's mechanical properties. By utilizing the materials elastic modulus variations, microcracks, defects, grain sizes and grain structures can be imaged by the UFM and provide a detailed qualitative image. By applying this AFM-UFM technique, the developers and manufacturers in the microelectronic industry have a method that can provide important device and component information quickly and with minimal sample preparation. The power of this technique has been demonstrated on three characterization application issues. The detection of microcracks in laser modified head sliders, the grain structure analysis of micron and sub-micron width copper microwires and an analysis of the grain boundary region in Al_2O_3-TiC substrate wafers were addressed.

ACKNOWLEDGEMENTS

This research effort was supported by the National Science Foundation (Grant CMS-9905394), DARPA NDE-MURI (Grant F49620-96-1-0442), School of Engineering at the University of Dayton (Enhancement Scholarship), Center for Materials Diagnostics (CMD) at the University of Dayton Research Institute (UDRI) and the Department of Materials Engineering at the University of Dayton. I would like to thank Prof. Daniel Eylon, Dr. Norbert Meyendorf and Mr. Edward Schumaker as well as all of the personnel at the Center for Material Diagnostics. Thanks also to Dr. Brar and Dr. Ganesh at the Seagate Corp. for allowing us to work with them and for their input and help along the way.

Very special thanks for his knowledge, insight and help along the way goes to my advisor, Dr. Sathish. His insight and direction during this thesis project made the undertaking a fantastic learning experience and a lot of fun.

TABLE OF CONTENTS

LIST OF FIGURES

List of Tables

CHAPTER 1

1.1) MOTIVATION

As a device's characteristic dimensions become small, the mechanical property of the component material may begin to deviate from bulk scaling laws. Deviations may occur when either the microstructural features (grain size) or object dimensions approach the length of scales of defects, defect interactions or processes that control deformation. While many material's physical properties may deviate from continuum models only at atomistic lengths scales, it is not uncommon for the material's mechanical properties to deviate from bulk scaling behavior at surprising large length scales. The mechanical property deviations can become apparent in the micrometer range, as is the case in thin films, micro and nano structures. So the bulk material mechanical properties may not be the same as the properties of the actual miniaturized device.

The goal of this study was to develop a material characterization technique that exploits the nanoscale imaging capabilities of the Atomic Force Microscope – Ultrasonic Force Microscope (AFM-UFM) to address current research issues with device miniaturization in the microelectronic industry. While the majority of material characteristics of microelectronic devices are measured through electrical and magnetic properties, the motivation of the present thesis

stems from the utilization of the elastic properties. Interaction of acoustic waves with defects in the bulk, surface and subsurface of material has been very effectively utilized in the field of nondestructive evaluation of materials. With the combined application of the Atomic Force Microscope and Ultrasonics, we expect to achieve detection and characterization of defects of nanometer size. The method has been successfully utilized on three different microelectronic applications; a) surface characterization and detection of microcracking in laser modified hard disc head sliders, b) grain size/structure characteristics in micron and sub-micron width copper wires and c) examination of grain boundary inhomogeneities in mechanically polished AL_2O_3-TiC substrate wafers. All three issues are technically challenging due to the extremely small area of interest and the desire for nondestructive analytical techniques with a fast analysis time. All three case applications can arise on a typical microelectronic device, by having one instrument and method capable of examining multiple items of interest is a further bonus of time and cost savings.

1.2) INTRODUCTION

State of the art electronic components are being manufactured in smaller dimensions with increasingly more intricate details. There are many applications where nanoscale imaging of a device can provide insightful and key information to the manufacturer about the state and operational condition of the material or device. Characterization techniques that produces high-resolution nanoscale images of micro and nano-cracks and provides information on grain sizes, grain structures, grain alignments, grain boundary interactions, defects and material changes occurring during usage, are increasingly important tools as device miniaturization occurs. The Atomic Force Microscope (AFM) is commonly used to provide nanoscale resolution on both conducting and non-conducting material in a wide variety of media [1]. The AFM has been widely used for the characterization of surface topography, friction, and wear on both hard and soft materials such as ceramics, metals and polymers [2-7].

The AFM is an extremely versatile instrument that was developed from the Scanning Tunneling Microscopy (STM). The AFM system consists of at least four basic hardware elements. These elements are a probe, a cantilever deflection detector, a scanner and the feedback electronics. The probe consists of two sections, the cantilever and the atomically sharp tip. The cantilever provides a support onto which the probe tip is attached. The cantilever and tip can be

manufactured from several different materials with various cantilever dimensions, tip shapes and spring constants depending on the intended material property or the integrity of the sample to be examined. The probe tip is attached a cantilever that can possess a spring constant weaker than the atomic bonds of the sample material so that the tip can lightly trace and not damage the sample surface. Typically commercially manufactured cantilevers are made from either silicon or silicon nitride. Figure 1 gives examples of the 2 basic cantilever layouts with Table 1 providing spring constants and resonant frequencies for common cantilever designs.

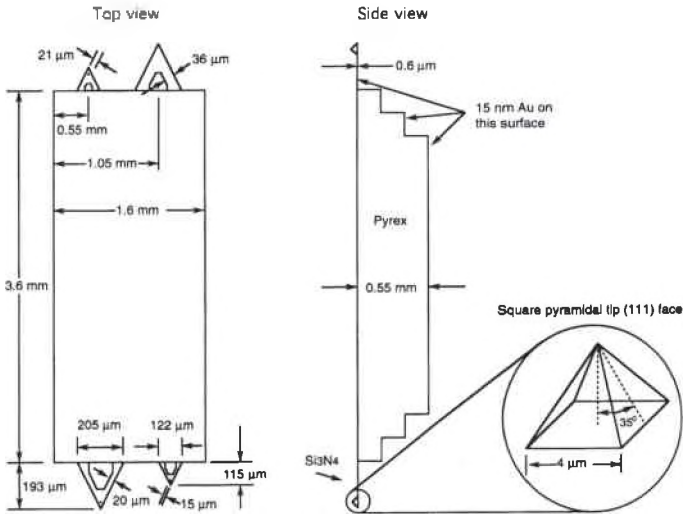

A) V-shaped Silicon Nitride AFM Tips

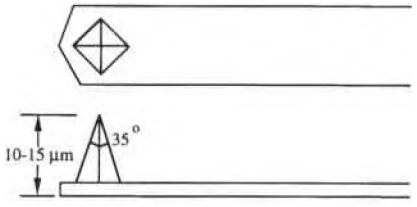

Contact AFM Cantilevers
Length = 450 μm
Width = 40 μm
Thickness = 1-3 μm
Resonance frequency = 6-20 kHz
Spring constant = 0.02-0.66 N/m

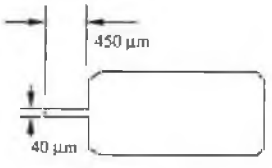

Tapping mode AFM Cantilevers
Length = 125 μm
Width = 30 μm
Thickness = 3-5 μm
Resonance frequency = 250-400 kHz
Spring constant = 17- 64 N/m

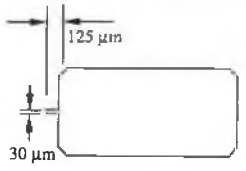

Material: Etched single-crystal n-type silicon;
resistivity = 0.01-0.02 ohm/cm
Tip shape: 10 nm radius of curvature, 35° interior angle

B) Rectangular Beam Silicon AFM Tips

Figure 1: Typical Cantilever/Tip Dimensions
[Bhushan, B., "Handbook of Micro/ Nano Tribology:" CRC Series Mechanics and Material Science, CRC Press, New York, pp.34-35 1995.]

Measured Vertical Spring Constants and Natural Frequencies of Triangular (V-Shaped) Cantilevers Made of PECVD Si_3N_4

Cantilever Dimension	Spring Constant (k_z), N/m	Natural Frequency (ω_0), kHz
115-μm long, narrow leg	0.38	40
115-μm long, wide leg	0.58	40
193-μm long, narrow leg	0.06	13–22
193-μm long, wide leg	0.12	13–22

Data provided by Digital Instruments Inc.

(A) Vertical Spring Constants and Natural Frequencies of Rectangular Beams Made of PECVD Si_3N_4

Cantilever Dimensions μm			Vertical Spring Constant (k_z) (N/m)	Natural Frequency (ω_o) (kHz)
L	W	T		
100	10	0.6	0.08	66
100	20	0.6	0.17	66
100	10	0.3	0.010	33
100	20	0.3	0.021	33

Note: $k_z = EWT^3/4L^3$, and $\omega_o = [k_z/(m_c+0.24WTL\rho)]^{1/2}$ where E is the Young's modulus, m_c is the concentrated mass of the tip, and ρ is the mass density of the cantilever (Sarid and Elings, 1991). For Si_3N_4, E = 150 GPa and ρ = 3100 kg/m³.
Data provided by Park Scientific Instruments.

(B). Vertical (k_z), Lateral (k_y), and Torsional (k_{yT}) Spring Constants of Rectangular Cantilevers made of Si (IBM) and PECVD Si_3N_4

Dimensions/Stiffness	Si Cantilever	Si_3N_4 Cantilever
Length (L), μm	100	100
Width (W), μm	10	20
Thickness (T), μm	1	0.6
Tip length (l), μm	5	3
k_z, N/m	0.4	0.15
k_y, N/m	40	175
k_{yT}, N/m	120	116

Note: $k_z = EWT^3/4L^3$, $k_y = EW^3T/4l^3$, and $k_{yT} = GWT^3/3l^2$ where E is Young's modulus and G is the modulus of rigidity [= E/2(1 + ν), where ν is the Poisson's ratio]. For Si, E = 130 GPa and G = 50 GPa.

Table 1: Spring Constants & Resonant Frequencies for Common Cantilevers
[Bhushan, B., "Handbook of Micro/ Nano Tribology:" CRC Series Mechanics and Material Science, CRC Press, New York, pp.34-35 1995.]

As the tip engages the sample surface the cantilever will deflect based on the forces acting on the tip. Monitoring the cantilever deflection is how the AFM measures the surface height or forces. There are several different methods for measuring the deflection of the cantilever. In this study the AFM system measures the amount of cantilever deflection by reflecting a laser beam off of the cantilever's back surface into a four quadrant laser diode detector. The photodiode detector can measure minute changes in the laser deflection as the probe tip is scanned across the sample. The laser deflecting off of the cantilever into a photodiode precisely measures the cantilever deflection allowing for angstrom resolution.

The third component in the basic AFM system is the probe scanner. The scanner is constructed out of a combination of piezo electric materials. Piezo material allows precise control of the motion of the tip in the X, Y, and Z directions across the sample. All piezo material exhibits some nonlinearity and hysteresis, but these effects can be compensated for through the electronics and calibration of the scanning device. AFM systems can have the scanning piezoelectric installed in the tip head or below the sample stage. Depending on the location of the scanner, either the sample or the probe head will be raster scanned during imaging. In this study, the AFM system has the scanner moving the probe head with the sample being stationary.

The fourth element in a basic AFM system is the feedback electronics, which control the sample tip interaction. The AFM can be operated in three basic modes, contact, intermittent or tapping mode. Contact mode can be operated in

either constant height or constant force mode. In constant force mode, the surface topography is measured, while in constant height mode the interaction forces (repulsive/attractive) between the sample and tip are measured. In constant force contact mode operation, the feedback electronics maintains a set force between the sample and tip (i.e. same cantilever deflection). The AFM feels the topography of the sample surface under the nanometer sharp probe tip. When the tip in counters a high surface asperity the cantilever deflection will increase, so the feedback electronics will raise the z height to return the cantilever deflection back to the preset point. The system electronics use a feedback loop to maintain the cantilever deflection by continually adjusting the z height as the sample is scanned in the x and y direction. A surface topography image is outputted by correlating, point by point, the x and y scan position of the tip with the z height measurement of the scanner.

The lateral resolution of atomic force microscope and all scanning probe microscopes is based on the probe tip diameter. By manufacturing a smaller, sharper tip, the resolution can be increased. This allows AFMs to obtain extreme magnifications ranging from 10^3 to 10^9X in x, y, and z direction [1]. This magnification ability surpasses the Scanning Electron Microscope (SEM) and Transmission Electron Microscope (TEM) that have 10^7 magnification. The SEM and TEM are based on the properties of electrons. Though electrons are extremely small particle, one must remember that by quantum physics, electrons are energy waves and the lateral resolution issue of 2 waves is again a limiting resolution. Also the AFM instrument can record data in a multitude of sample

environments such as ambient air, various gases, liquid, vacuum, and cryogenic to high temperature [1].

With advances in modern manufacturing, the topography variation on a microdevice's surface in the testing area of interest may be so minimal that the AFM surface topography images may lack contrast. An image consisting of a few square microns may provide little information and appear to be blurred due to the lack of topography changes even though the larger overall surface is quite rough. Though conventional AFMs only measure the surface topography, its nanoscale measuring capabilities can be exploited by other adaptations to the system. In recent years several new techniques, designs, and upgrades based on the Atomic Force Microscope platform have been developed that are capable of measuring mechanical, optical and thermal properties in the nanometer regime. Ultrasonic Force Microscopy (UFM) belongs to such a category and is capable of imaging elastic properties of materials at the nanometer scale.

Elastic property imaging with microscopic resolution for material characterization is usually performed using Scanning Acoustic Microscopy (SAM). SAM is an evaluation technique based on the materials elasticity that is frequently used for nondestructive evaluation of materials. However Acoustic Microscopy requires a coupling medium to bring the acoustic waves into focus and its lateral resolution is limited by the wavelength of the acoustic waves in the coupling medium. Thus, the application of acoustic microscopy to the nanometer regime is very difficult due to the limitation of spatial resolution and the need for a coupling fluid. In order to overcome this limitation, the Ultrasonic Force

Microscope (UFM) has been developed. The UFM is a near-field microscope, which overcomes the resolution limit of the traditional acoustical microscopy and allows elasticity mapping of the sample without the need for submerging the sample in a coupling fluid/medium.

The addition of the Ultrasonic Force Microscope (UFM) to the AFM provides a valuable asset to the scientist or engineer seeking to investigate material interactions on the nanoscale regime. At the nanoscale level, the UFM utilizes the point of the AFM probe tip to sense the ultrasonic displacements generated by propagating an ultrasonic wave through the material. The AFM-UFM's resolution is determined by the diameter of the probe tip with the tip's amplitude response being directly related to the elastic modulus of the material under the tip. Therefore it is possible for an AFM to image elastic properties with very high spatial resolution.

The UFM records the contact stiffness between the sample and the AFM probe tip. By sensing the elasticity variations directly below the tip, the contact stiffness data measured by the UFM can be used to evaluate several material characteristics. The contact stiffness measurement can aid in detection of micro and nano cracks, grain sizes and structures, grain boundary inhomogeneities, material defects and other surface and subsurface material changes that can not be clearly distinguished with the conventional AFM.

1.3) AFM-UFM TECHNIQUE: EXPERIMENTAL PROCEDURE

A Digital Instruments Dimension 3000 Nanoscope IIIa AFM has been used to characterize the surface topography. The AFM was modified to measure the surface displacements generated by propagating an ultrasonic signal through the sample in order to examine the near surface elastic properties of the material (Ultrasonic Force Microscopy). There are several different methods of combining ultrasonics with the AFM [8-12]. These methods differ by the regime of operation, linear or nonlinear response, along with the ultrasonic excitation method and location of the transducer signal. In our investigation, the AFM was configured in conventional contact mode with the transducer placement as shown in Figure 2.

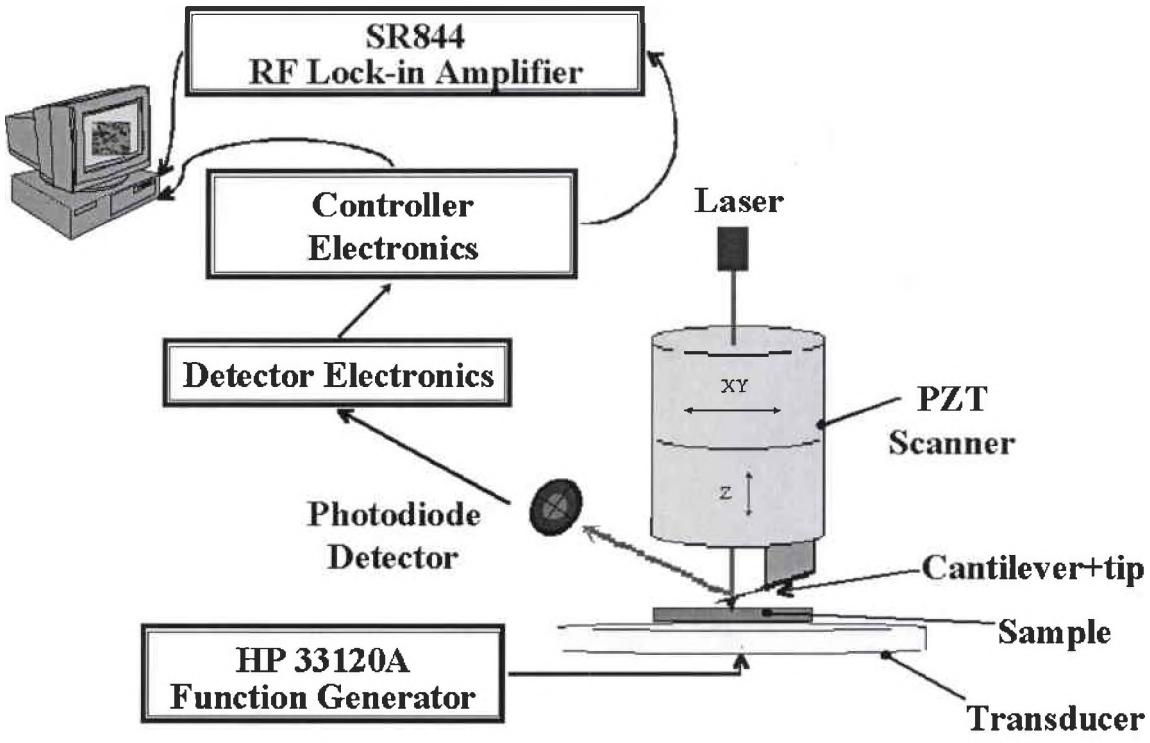

Figure 2: Schematic of UFM Equipment

For propagating the longitudinal ultrasonic wave through the sample, a piezo-electric transducer was bonded underneath the sample. The peizo electric transducer received its input from a Hewlett Packard function generator (HP Model #33120A) and generated a low amplitude continuous wave radio frequency signal in the range of 300 kHz to 1 MHz. The opposite side of the sample surface is in contact with the AFM probe tip. The AFM probe tip was utilized to detect and map the surface displacements generated by the longitudinal acoustic wave. Both AFM and UFM images can be acquired simultaneously on the same region. The simultaneous image acquisition was achieved by using the electronic feedback signal from the AFM's topography image and feeding it through a filtering and separating electronic loop. The

electronic filtering loop was used to separate the ultrasonic image (high frequency) from the surface topography (low frequency). A lock-in amplifier (Stanford Research Systems Model # SR844RF) is used to measure the amplitude and phase of the detected ultrasonic response signal with respect to the input signal from a function generator (Hewlett Packard Model #33120A). The amplitude or phase data was then transferred to the controlling computer and correlated with the scanning point to generate the ultrasonic image.

The AFM topography images were acquired in standard contact mode AFM as per the instruments operating instruction. [13] The UFM configuration required both the amplitude and ultrasonic frequency to be optimized. After the AFM had lowered the probe tip and successful engaged the sample surface, a force curve would be acquired and the force setpoint adjusted to a suitable minimum. With an acceptable force curve acquired, then the ultrasonic frequency for imaging had to be selected. The optimization was performed by two different methods.

In the first method the amplitude and the frequency of the input signal were manually varied and the output signal of the lock-in-amplifier was monitored for the maximum stable transmission signal. Several precautions had to be taken in selection of the ultrasonic frequency. Too high of a power input into the transducer could cause the AFM tip to bounce off of the sample surface resulting in streaked or unrepresentative images. The optimum frequency would allow a high amplitude response while maintaining a stable signal due to a low transducer input voltage. On most samples, three or four different frequency

points in the range of 400-1000 kHz were found to produce significant amplitudes and a stable response that are suitable for imaging.

In the second approach, a network analyzer (Hewlett Packard, Model #8753D) was employed. The transducer was connected to the input side and the AFM system feedback output was connected to the output end of the network analyzer. The analyzer treats the entire system as a two-port network and the entire frequency range could be checked automatically. The best transmission frequency was recorded and then used to set the function generator conditions. Although the second method was quite fast, it gave the same conditions that were obtained with the manual tuning method.

With the suitable ultrasonic frequency selected, a sample scan would be started. During the 1^{st} scan after sample engagement, the feedback controls would be adjusted as necessary. The feedback controls allowed the force setpoint, integral gain, proportional gain or look ahead gain to be adjusted to keep the tip in constant contact with the surface during scanning.

1.4) Elasticity Contrast at Nano Scales

There are two primary ways that material property data can be collected from the tip sample interaction with the AFM. One way is a quasi-static data acquisition where a force curve is recorded at a single point. The data is a plot of the tip sample interaction forces as a function of the tip height position. This method is time consuming and requires large data storage. The second method collects material property data using a modulation technique. The image is generated from the cantilever's amplitude or phase motion, while either the distance between the cantilever and sample or the force applied to the sample is modulated. The cantilever's amplitude response at a specific penetration depth is proportional to the slope of the force penetration depth curve at that particular depth. The power of the second method is in the ease with which an image of inhomogeneous materials is acquired.

In scanning probe microscopy techniques, contact can be defined as the point on the force separation distance curve at which there is a detectable repulsive component to the tip sample interaction. In contact with the sample, both attractive and repulsive forces contribute to the interaction force between the tip and sample. The interaction stiffness k_i is a force gradient. It can be measured at any tip sample separation or penetration depth. If the sample is

strongly loaded or if the attractive forces are negligible then the role of the attractive force can be ignored in the value of k_i (it is mainly repulsive force, the sample pushing back on the tip).

The local surface topography, the probe tip's size and shape strongly influence the contact stiffness measurements. The tip-sample interaction can be modeled by a Hertzian contact as shown in Figure 3.

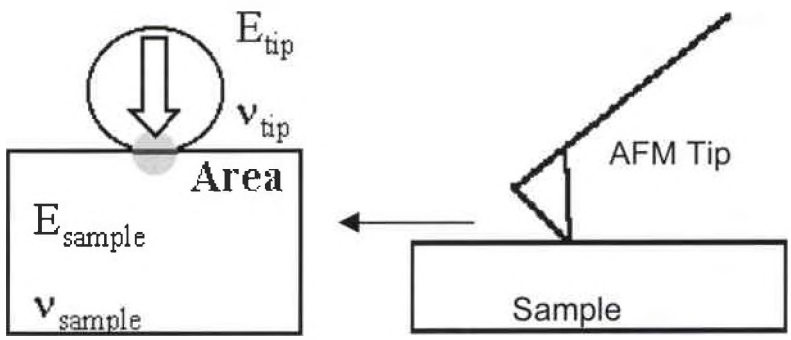

Figure 3: Interaction Stiffness defined with a Hertzian contact

The interaction stiffness can be related to material properties such as Young Modulus. In the limit of negligible adhesion and if a spherical probe tip is employed, the interaction stiffness can be defined as in equation 1. [14]

$$k_i = \frac{3 * a * K}{2} \qquad \text{(Eqn-1)}$$

k_i is the interaction stiffness

where K is the reduced modulus for the tip and sample and

a is the contact radius between the tip and sample

The Poisson ratio *v* and Young's Modulus E are used to define the reduced modulus K. The reduced elastic modulus is given in equation 2.

$$\frac{1}{K} = \frac{3}{4}[(\frac{1-\nu_{tip}^2}{E_{tip}}) + (\frac{1-\nu_{sample}^2}{E_{sample}})] \qquad \text{(Eqn-2)}$$

where v is the Poisson Ratio ($-\varepsilon_x/\varepsilon_z = -\varepsilon_y/\varepsilon_z$)

E is the Young's modulus

Assuming that the Young Modulus of the tip and the Poisson Ratio are constant during scanning, variations in the modulus of the sample can be imaged. While imaging the AFM feedback seeks to maintain a constant light setpoint force on the sample surface. With the tip force on the sample being maintained constant, the Poisson ratio of the tip as a consequence should not change. The Poisson's ratio for the sample may be changing slightly since it is a function of the sample elasticity. So in the reduced modulus equation for the tip and sample, the only factor changing is the E_{sample}. that is in the right hand term in equation 2. Thus the interaction stiffness changes in the image can be directly attributed to the changes in the stiffness of the sample.

It is also assumed that over the course of one image scan, the probe tip is not degrading and the contact area is not increasing. On first engagement with the sample surface for a scan, the probe tip point may dull slightly when the nanometer sharp tip end comes into initial contact with the surface. From the start of data collection to the end of 1 image scan, it is assumed that the tip contact area is maintained constant. To validate the assumption that the tip diameter is constant during the scan, repetitive images were collected. The

structure resolution was checked to make sure that it was not changing from scan to scan which would indicate that the tip sample contact area was also changing during the scan. If the resolution of the imaged structure degraded upon subsequent imaging, a new sensing tip would have been installed. Dust debris or dirt from the sample surface did occasionally accumulating on the probe tip resulting in an increased contact area/ or force input and streaks or blurred lines in the image. If streaking or other artifacts appears in the images, the sample would be rescanned with a new tip.

Assuming that the tip diameter, tip elasticity, Poisson ratio are maintained constant during the data scan collection, the only variable changing in the contact stiffness equation that is sample elasticity. So the UFM image can be considered a map of the elastic stiffness of the material under the tip. The change in contrast in the UFM image is directly caused by these elastic modulus variations in the sample below the tip. It is also believed that the depth sensitivity of the UFM is several times the diameter of the tip [9]. Hence the information contained in the UFM image is an averaged value from the top layers of the surface over a thickness of several times the tip diameter. For low amplitude ultrasonic excitation, the AFM tip is expected to be in contact with the surface and the surface displacements detected by the AFM tip are directly proportional to the stiffness of the material under the tip [9,15]. The discussion presented above is qualitative in nature, but provides a simple physical explanation of the contrast in the UFM images. Burnham et al. has developed a more elaborate rheological model for Ultrasonic Force Microscopy. The model shows that the amplitude

detected by the AFM tip is proportional to the elastic stiffness of the material underneath the scanning probe tip [9,15-16]

Burnham et al. proposed the model shown in Figure 4 for the tip sample interaction when the excitation force is a low amplitude sinusoidal function.

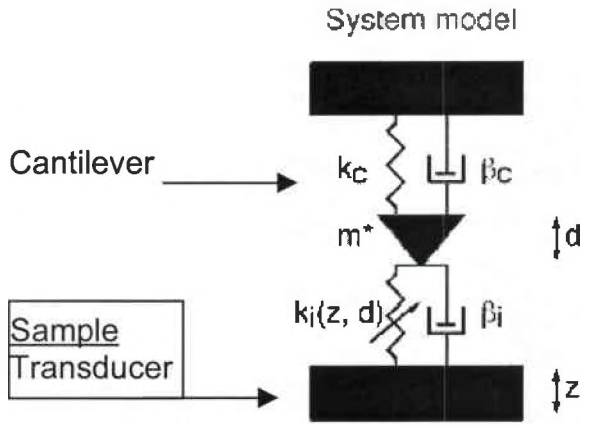

Figure 4: Model Proposed by Burnham et al. for Tip-Sample Interaction
[Burnham, N., Kulik, A.J., Gremaud, G., Gallo, P.J., and Oulevey, F. "Scanning local acceleration microscopy", *Journal of Vacuum Science and Technology*, Vol. 14, No. 2, pp. 795, 1995]

The position of the sample and cantilever is shown above. The sample would be sitting on top of a transducer. In this model the cantilever spring stiffness is represented by k_c, the damping constant is β_c, and the effective mass is m^*. The sample-tip interaction stiffness is $k_i(z, d)$ and its damping is $\beta_i(z, d)$. If contact is occurring in the presence of low adhesion forces or high loads then $k_i(z, d)$ can written as

$$k_i(z,d) = \frac{3 * K * a}{2} \qquad \text{(Eqn-3)}$$

It is assumed that the excitation amplitude is small enough and that the AFM feedback loop is maintaining a constant load (i.e. AFM is in constant force not constant height mode) then

$$k_I(z, d) \Rightarrow k_I \quad \text{and} \quad \beta_I(z, d) \Rightarrow \text{is } \beta_I \qquad \text{(Eqn-4)}$$

The interaction is assumed to be largely elastic so that the interaction damping is low. These assumptions allow the model to be solved analytically. The expressions for the position of the transducer and the cantilever and the equation of motion for the system are

$$z = z_0 + z_1 \cos \omega t \qquad \text{(Eqn-5)}$$

$$d = d_0 + d_1 \cos (\omega t - \delta) \qquad \text{(Eqn-6)}$$

$$m^* \ddot{d} + 2m^* \beta_c \dot{d} + k_c d = 2m^* \beta_i (\dot{z} - \dot{d}) + k_i (z - d) \qquad \text{(Eqn-7)}$$

The subscript 0 denotes the dc component while the subscript 1 denotes the ac components of the z and d terms. The ac cantilever response amplitude divided by the ac transducer excitation amplitude can be solved for from equations 5-7.

$$d_1/z_1 = k_I[1 + (2m^*\omega\beta_I / k_I)2]^{1/2} / \{(k_I + k_c - m^*\omega^2)^2 + [2m^*\omega(\beta_I + \beta_c)]^2\}^{1/2} \qquad \text{(Eqn-8)}$$

The ratio d_1/z_1 is plotted as a function of normalized frequency relative to the cantilever resonant frequency (ω) and as a function of k_I relative to k_c.

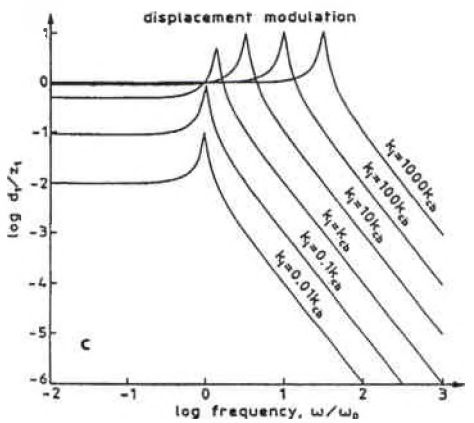

Figure 5: Plot of Frequency Versus d_1/z_1 Illustrating Point of Contrast Inversion

[Burnham, N., Kulik, A.J., Gremaud, G., Gallo, P.J., and Oulevey, F. "Scanning local acceleration microscopy", *Journal of Vacuum Science and Technology*, Vol. 14, No. 2, pp. 795, 1995]

If an operational frequency is chosen within the region of resonance contrast inversion can occur. Contrast inversion occurs when portions of the lower valued k_i/k_c are above some of the higher valued k_i/k_c curves as seen in Figure 4 [9]. As a result of contrast inversion only qualitative difference in elasticity can be inferred. From an image, it can be stated that there is a difference in modulus between the two materials and not which of the materials has the higher modulus. (Though the qualitative information can provide characterization information on the grain size, microcracking, defects in the device). The phenomena of contrast inversion has been documented by two research groups [9,17].

Rabe et al have developed a similar theoretical model incorporating the higher order modes of vibration from the tip-sample. This allows interpretation of results obtained if measurements are preformed using one of the higher resonant frequencies of the cantilever [17].

This rheological model can, in principle, provide an explanation for different modes of operation and show frequency limits. If one looks at the region where force modulation or lower frequency modulation techniques are used, assuming low damping the low frequency limit is

$$\frac{d_1}{z_1} = \frac{k_i}{k_i + k_c} \quad \text{so if } k_i >> k_c \text{ then } \quad d_1/z_1 = 1 \qquad \text{(Eqn-9)}$$

For stiff samples, force modulation techniques will employ a stiff cantilever or a large amplitude modulation thereby either force sensitivity is compromised or the large amplitudes induced result in lateral sliding of the tip. So the lateral resolution is degraded and frictional effects can be combined into the image in force modulation.

The high frequency limit is

$$\frac{d_1}{z_1} = \frac{k_i}{m^* \omega^2} \qquad \text{(Eqn-10)}$$

The ratio of the response becomes linearly dependent on k_i and independent of the cantilever stiffness. Weak cantilever can be used on stiff samples and maintain force sensitivity while measuring mechanical properties. Ultrasonic Force Microscopy is operated at higher frequencies above the cantilever and resonance allows exploitation of the point that modulating at frequencies above the system resonance affords the clearest difference in cantilever response for variations in the elasticity of stiff samples.

This setup was chosen for its simplicity and for its ability to directly relate the ultrasonic response to the sample elasticity in the linear response regime. For

imaging stiff materials, the ultrasonic frequency employed was well above the resonance frequency of the cantilever, which allowed the use of weak cantilevers for good force resolution and property measurements. These facts help in attributing the contrast in the UFM image to the elastic property variation in the material.

CHAPTER 2 -MICROCRACK DETECTION

2.1) Composite Head Sliders

In a computer Hard Disc Drive (HDD), the read/write chip that flies over the surface of the magnetic storage disc is known a head slider. The head slider is a tiny composite device (1mm x 1mm x 0.3 mm).

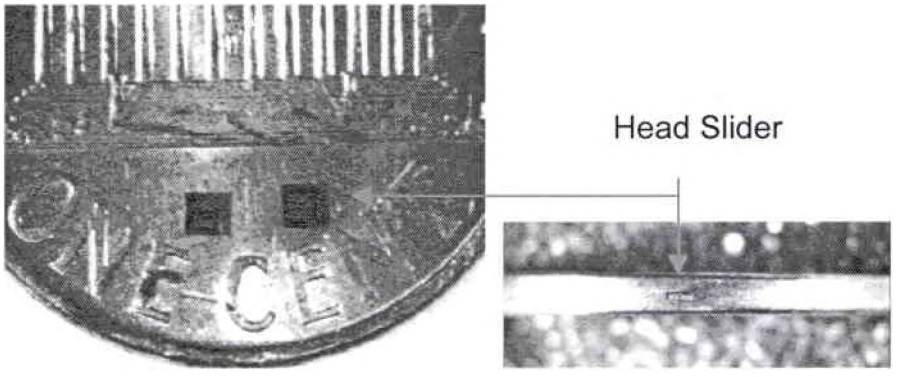

Figure 6: Size of Head Slider Chip in Reference to the U.S. Penny Coin

The head slider is responsible for writing or reading the magnetic bits to and from the hard drive. The typical head slider consists of an Aluminum Oxide-Titanium Carbide composite body, two layers of magnetic Permalloy film, a conductive copper coil, and an amorphous alumina overcoat and gold electrical connections [18]. Located on one end of the slider in the amorphous alumina overcoat is the pole tip region where the magnetic layer and conducting coil are configured to read and write the magnetic bits. Carved into the underside of the

Al2O3-TiC body are the Air Bearing Surface (ABS) rails responsible for the flight characteristics. Figure 7 illustrates the basic chip layout and location in your computer hard drive.

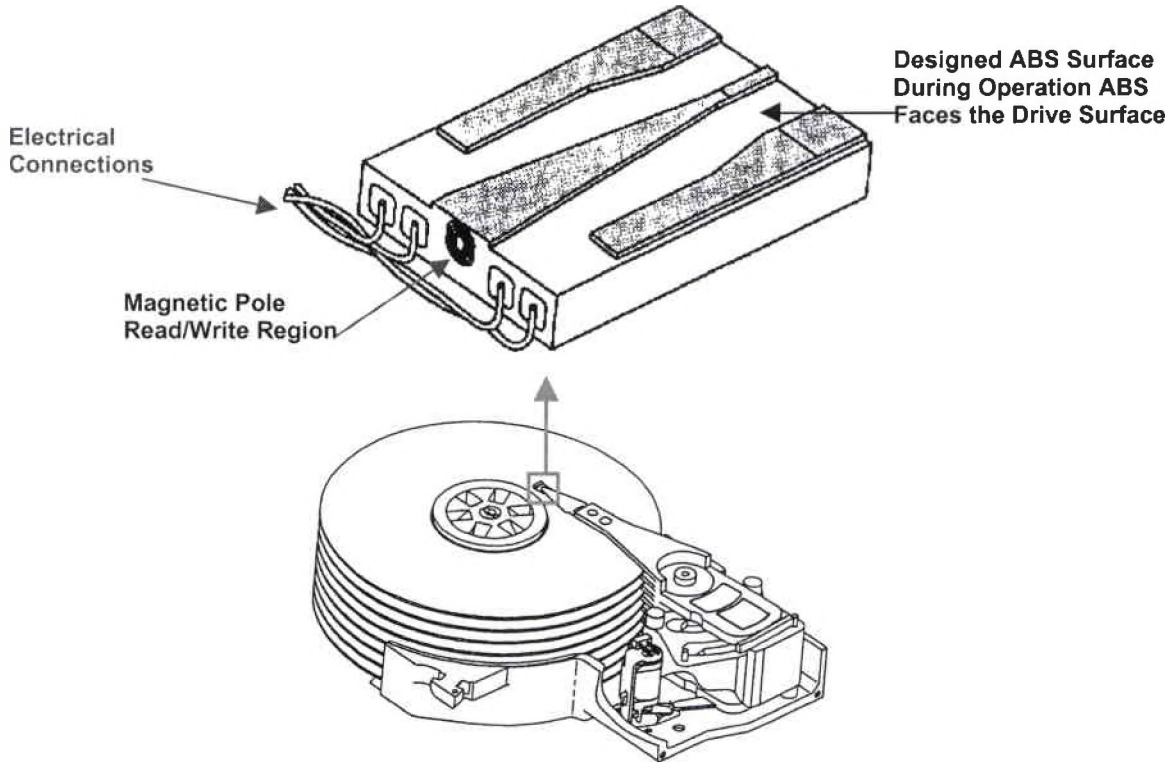

Figure 7: Typical Head Slider Schematic

[Bhushan, B., "Handbook of Micro/ Nano Tribology:" CRC Series Mechanics and Material Science, CRC Press, New York, pp.66-7 1995.]

In order to produce magnetic storage densities exceeding 10Gb/in^2 in a computer hard drive, several characteristics of the drive components have to be optimized. The requirements for higher storage densities have led to the development of miniaturized read/write head sliders that fly over the magnetic disc storage surface with very low flying heights, the distance between the hard drive and the head slider. First generation head sliders in the early 1980's were

4mm long x 3.2 mm wide and almost 1mm thick whereas today's Femto sliders measure a mere 0.85 mm (L) x 0.7mm (W) 0.23mm (T)[18-19]. Other requirements for increasing storage density include the use of supper smooth hard discs and specially sculptured slider surfaces. These new component designs have posed new technical challenges for material characterization methodologies.

Miniaturized sliders allow greater disk utilization, lower disc separation, more sliders per wafer, enhanced shock performance, improved response to disk waviness/asperity and improved tribological performance [19]. With the reduction in slider size, the flying heights above the magnetic disk surface have been reduced to 20 nm. or lower. At such small distances the flying altitude must be extremely stable to avoid contacting the hard disk surface. In order to have precise flying characteristics, the bottom surface, the Air Bearing Surface (ABS), of the chip has a specially designed configuration. Depending on the type of slider the ABS surface configuration can be designed to induce a positive pressure or negative pressure flying effect. Since the slider is a composite, during or after construction the device may need very fine adjustments or shaping of the ABS crown depending on the crown angle and shape. These desired adjustments maybe as small as only a few nanometers [20].

2.2) Modification of Slider Surfaces

To precisely control the surface structures of head slider and other hard drive components, various techniques of surface preparation such as mechanical

abrasion, chemical etching, ion milling or laser tooling/treatments are utilized. Among these techniques laser tooling offers several key advantages. It is non-contact, abrasion less, eliminates chemical etchants, and eliminates problems associated with mechanical tools like wear, vibration, deflection and cutting forces. In addition, laser tooling reduces the limitations on structure formation [21]. Laser tooling has been used on computer disc drive components to create surface texture for the reduction of stiction, to remove sub-micron debris or organic films, and for adjusting the surface crown of the head slider in order to improve the slider's flying characteristics [20].

Treatment of a head slider is significantly different than the more common technique of texturing the landing zone of hard disk surfaces because of the composite nature of the sliders. High hardness, modulus and optimum toughness of the ceramic, Al_2O_3-TiC used in the slider construction can make it difficult to perform such fine adjustment by mechanical methods especially while working on a device with a surface area of the order of a square millimeter. Techniques such as laser cleaning, ion beam etching, and laser curvature adjustment technique (LCAT) have been shown to be very promising for modifying the slider surfaces [20-27]. Although laser tooling has several advantages is can produce high temperature gradients, leading to the development of large residual thermal stresses that can cause cracking in ceramic material. Cracking in the ceramic material can cause the components to malfunction [21,22,28].

2.3) The Need for Microcrack Detection

Observation of microcracks in such nano-composite materials is a difficult task. The multiphase ceramic composite materials used in the head sliders have an average grain size of the order of one micron. Standard optical microscopes are fundamentally limited by optical diffraction to 0.2 μm resolution. Scanning Electron Microscope (SEM) can be used but extensive sample preparation is needed. Also picking out the microcracks from the surrounding surface can be a major challenge. It can be difficult to differentiate between a crack and a scratch both in the optical microscope and the SEM.

The Scanning Acoustic Microscope (SAM) is very efficient in detecting surface and subsurface cracks due to the nature of the interaction of the acoustic wave with the crack. But SAM's lateral resolution is limited by the acoustic wavelength and its application requires a coupling medium usually water. It is well known that an acoustic wave interacts with cracks and provides a way to detect their presence in the material. When an AFM tip is utilized to detect the surface displacement caused by a propagating acoustic wave. We expect to observe differences in the response amplitude in the vicinity of a crack and away from the crack. This additional information is expected to play an important role in the detection of cracks much smaller than a few microns.

One of the most powerful tools that is routinely used for characterization of nanostructured materials is the Atomic Force Microscope (AFM). Conventional AFM and modified AFMs have been used for characterization of surface

topography, friction and wear properties of head sliders and hard disk materials [6,29-32]. While most of these studies have been performed on neat head slider materials, very few studies have been reported on laser surface modified devices. In a study on magnetic thin film heads of alumina, Chekanov et al. has reported observation of cracks generated due to thermal fatigue and contact in the pole region [30-31].

The ability to characterize the laser treated surface is very important in order to optimize the tooling conditions so that the sliders are produced free of thermally induced stresses and cracks. This technique allows imaging of both the surface topography and the elastic property variations at nano-scales. The surface topography data from the AFM is not always able to provide the necessary details about the material changes that have occurred due to the laser treatment. Substantial material changes may be hidden or obscured within the topography data in areas of either little or major surface topography variations. The UFM by focusing on the modulus of elasticity changes is able to uncover or highlight the material changes that may be missed in the AFM data. For the AFM measurement the probe tip is only riding on the sample surface measuring height where as in the UFM an ultrasonic wave is interacting with the sample material allowing material property information to be collected. The interaction between the acoustic wave and the sample elastic variations in turn give the image a better contrast and enhanced detection and visibility of microcracks, individual material grains and surface micro-structural features. This combination technique

of UFM allowed microcracks to be clearly distinguished and detected better than the existing method used by the manufacturer.

2.4) Devices Studied

The bodies of the head sliders examined in this investigation are composites mainly of Al_2O_3-TiC. The approximate composition is 70% Al_2O_3 and 30% TiC with an average grain size of the material is in the range of 1 micron. The dimensions of the slider chips examined were 1.3 mm x 1.0 mm with a thickness of 0.3mm. Sections of the slider's back face, opposite of the ABS surface were modified with a laser in order to modify the crown on the air bearing surface. Processing details concerning the laser adjustment technique employed for the crown adjustment on the head sliders were not disclosed.

Ten head sliders subjected to laser modification were surface characterized by the AFM-UFM technique. The sliders had been subjected to the laser surface treatment in order to adjust their crown angle. The devices were cleaned in de-ionized water and dried with acetone. Each of the sliders was mounted on the ultrasonic transducer with a tiny drop of honey in between the transducer and the slider. Honey was used to adhere the transducer and couple the ultrasonic waves to the sliders. The surface region scanned for slider analysis varied from 50 × 50 μm down to 500 × 500 nm with the scanning speed usually between 0.5 and 1 Hz. The ultrasonic images were captured at frequencies ranging from 450 kHz up to 905 kHz. V-shaped silicon nitride cantilevers with a spring constant of 0.12 were used for the measurements

2.5) Microcrack Results

Laser Treated Slider Surfaces

Typical results from three of the ten head sliders, (Slider #1, Slider #2, and Slider #3), are presented. Figure 8 shows sections of the laser modified surface on Slider #1 obtained using the optical microscope attached to the Atomic Force Microscope. The triangular object in Figure 8 is the AFM cantilever, which has the sensing tip located near its end. The diagonal parallel lines in the image are the result of the laser scans on the ceramic slider surface. A small portion of untreated region is also visible lying between two laser treated sections.

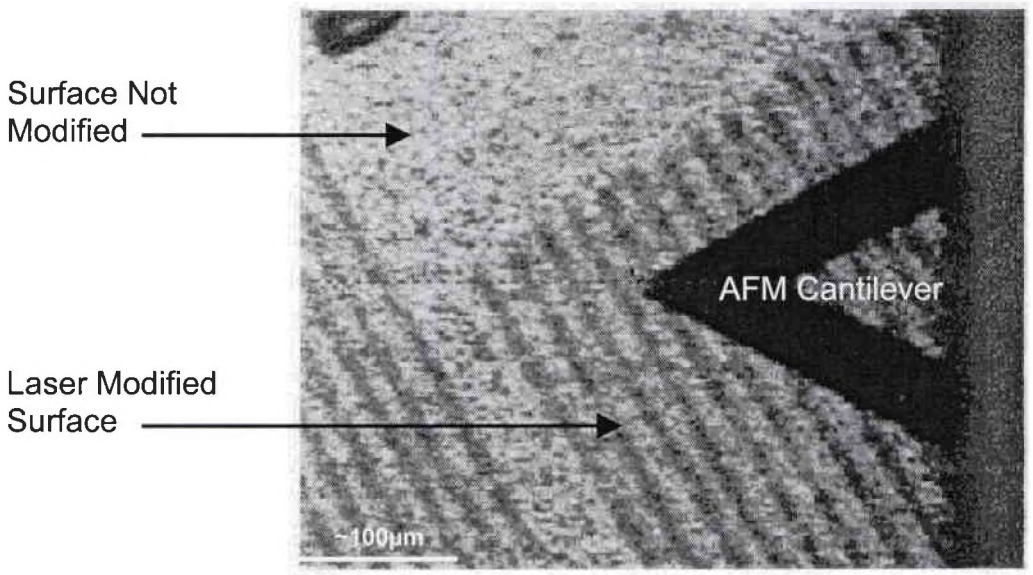

Figure 8: Optical Image of a Section of the Laser Shaped Surface

Characterization analysis was started by first scanning a large area of 50 microns x 50 microns. Subsequent higher magnification images were acquired to characterize the specific selected features of interest in the larger scan. Though many chip sections were examined only a few representative images will be

presented. The AFM and UFM images taken on the exact same area are presented side by side for comparison. In order to highlight the excellent crack detection ability of this method, two data image sets recorded on different laser modified sections will be compared and the similarity of the UFM responses discussed.

Figure 9 shows both the AFM surface topography (Fig. 9A) and the UFM amplitude image (Fig. 9B) of the same region obtained in the middle regions of Slider #1. The maximum feature height in the surface topography image (Fig. 9a) is about 1 micron with several features reaching this height. The color scale bar in the upper left corner of both images can not be equated to one another. For the AFM topography image, the color bar scaling is representative of surface height in either nanometers or microns while the UFM scale bar is representative of received response signal in volts or millivolts.

Faint line-like features, indicating the presence of cracks are observed in the UFM's image (indicated by the arrows), but these same indicating features are buried within the AFM surface topography information. Attempts to improve the contrast of the AFM image while scanning the sample using online real time image enhancement procedures did not produce significant contrast enhancement. The UFM image (Fig. 9B) was acquired at an excitation ultrasonic frequency of 508 kHz. Many of the features observed in the surface topography image can also be observed in the UFM image with a better contrast.

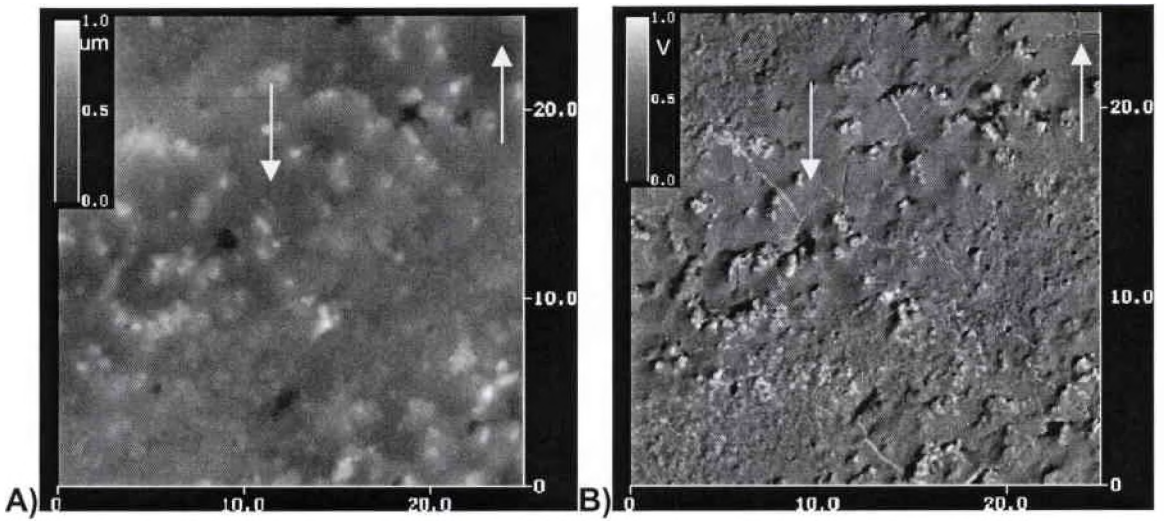

Figure 9: Laser Treated Surface on Slider #1

A) AFM surface topography image. B) UFM amplitude image

Scan area is 25 µm × 25 µm.

In order to characterize the features better, a smaller area of 15 µm x 15 µm in the region containing the faint features was imaged. Figure 9a and Figure 9b show respectively the AFM and UFM image of the magnified area. Even at this higher magnification identifying and locating the faint crack like features in the AFM surface topography image is not trivial. The UFM image (Fig. 10b) was acquired at an ultrasonic excitation frequency of 759 kHz and clearly shows a long crack almost diagonal to the image along with several other cracks originating from the main crack. It is observed that the long cracks appear to run along the grain boundaries.

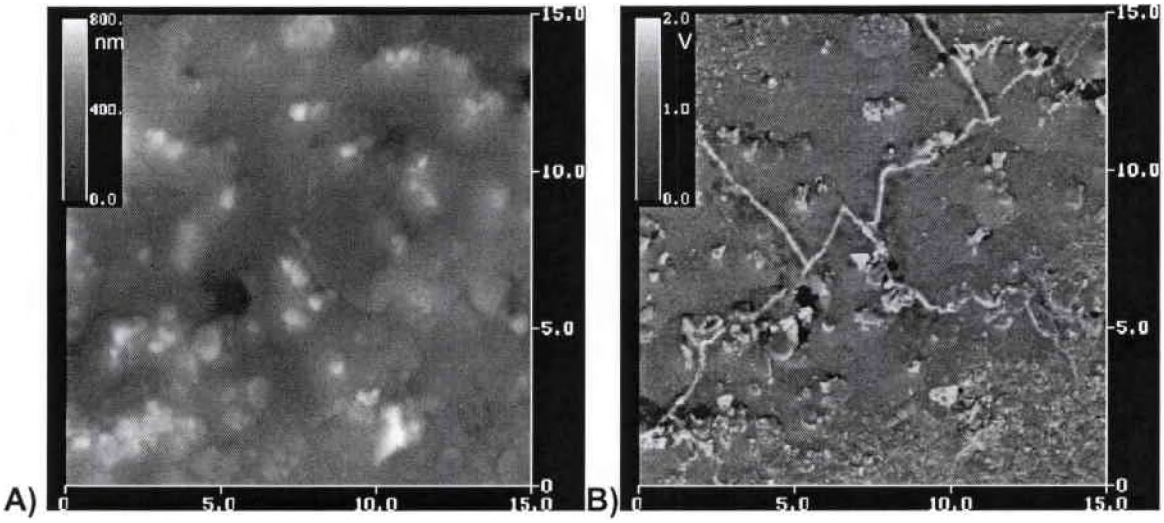

Figure 10: Higher Magnification Image of the Crack in Figure#9 on Slider #1
A) AFM surface topography image. B) UFM amplitude image
Scan area is 15 μm × 15 μm.

Another image set acquired in a different laser treated section of Slider #1 produced similar features as described above. Figure 11 shows both the AFM topography image (11A) and the UFM amplitude (11B) image acquired at an ultrasonic excitation frequency of 451 kHz in a laser treated section. Similar height features are present when compared to Figure 9, about 1 micron. The scale bar for Figure 11 AFM image is 0 - 775 nanometers in the AFM image. One can notice what appeared to be swaths with markedly less material protrusions from the surface and the protrusions are grouped in ridge of taller material across the image. In the UFM amplitude image (11B), there are similar line-like features indicating the presence of microcracks (again indicated by the arrows). These same features are buried and not distinguishable in the AFM information in figure 11A. Several crack paths are seen in this image.

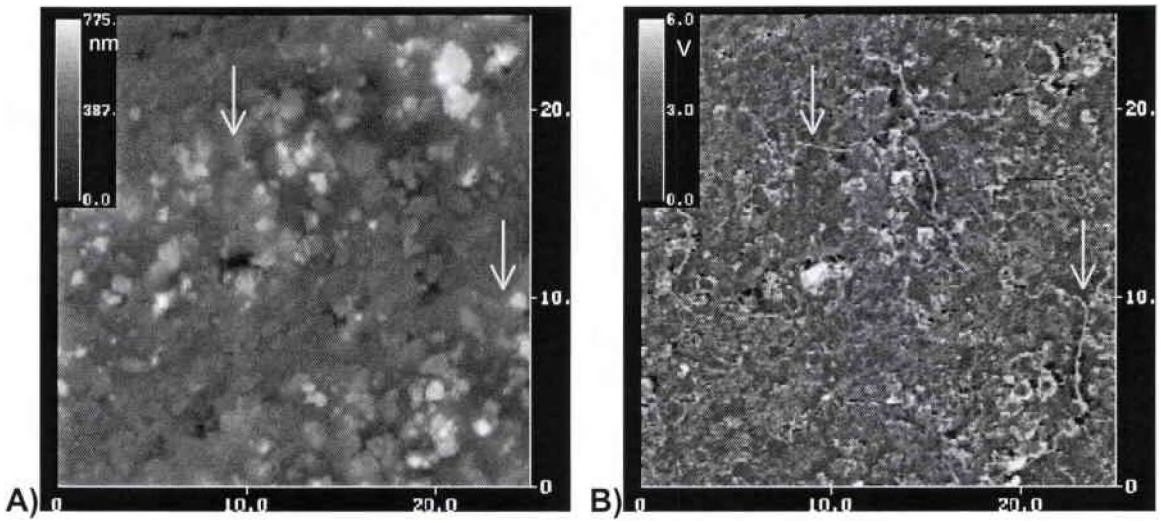

Figure 11: Second Analysis Location in Laser Treated Surface of Slider #1
A) AFM surface topography image. B) UFM amplitude image.
Imaged area is 25 μm x 25 μm.

Images at higher magnification on the same cracks in the lower right side of the UFM image in Figure 11 are presented in Figure 12 and Figure 13. Not only does higher magnification clearly shows the microcracking but a wealth of other details are brought forth in the UFM images. Figure 12 was acquired at an ultrasonic excitation of 451kHz while in Figure 13 the acquisition frequency was 741kHz. In Figure 12 and 13, new features other than the cracks are highlighted using the circles. It appears the grains in the laser treated region have gotten loose from the matrix.

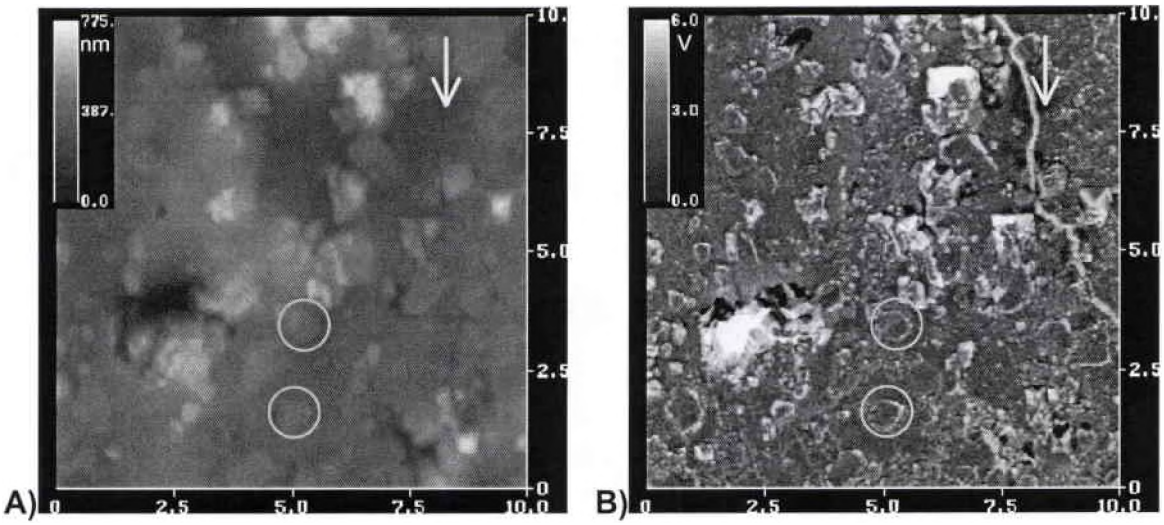

Figure 12: Appearance of Loosened Grains on Slider #1
A) AFM Surface Topography Image. B) UFM Amplitude Image.
Imaged area is 10 μm x 10 μm.

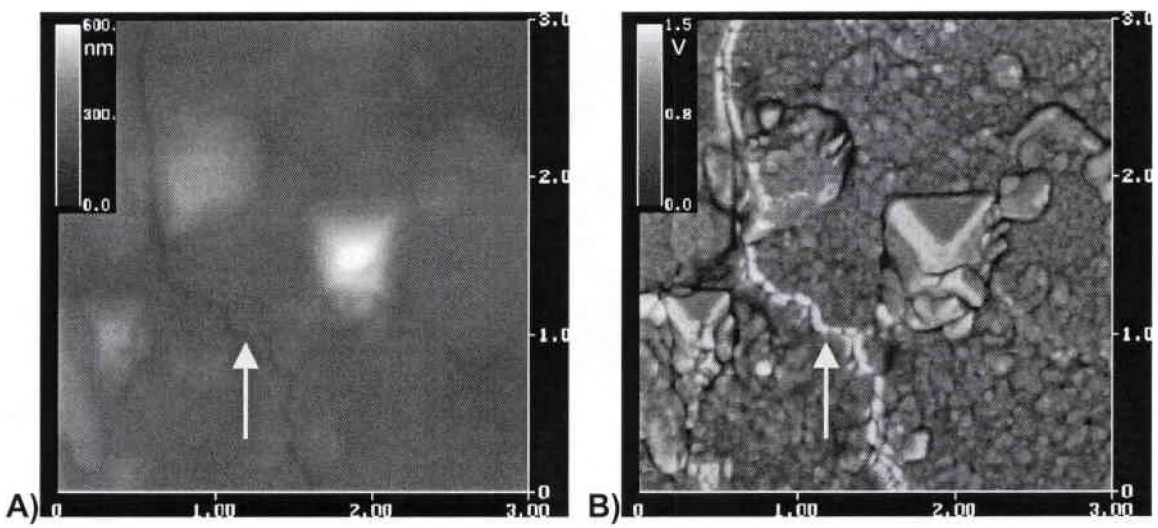

Figure 13: Appearance of Nano Droplets not Visible in AFM
A) AFM Surface Topography Image. B) UFM Amplitude Image.
Imaged area is 3 μm x 3 μm.

A comparison of the AFM images at different magnification shows that only at very high magnifications are the crack features observed. On the other hand these features are evident in the very first low-resolution UFM images. The

cracks in the UFM image have bright features around them. Also highlighted in the circles in Figure 12 are substrate grains that have been loosened from the surface. In both locations, the cracks are distinctively highlighted from the rest of the surface.

Figure 14 shows surface topography AFM (Fig. 14a) and UFM amplitude image (Fig. 14b) acquired at 905 kHz on laser treated region of Slider #2. As it has been observed earlier, the AFM image does not exhibit appreciable contrast in order to see the cracks among the surface height variations. On the other hand, the UFM image clearly indicates the presence of the microcracks as well as the morphology of the grains. Another interesting feature that can be observed in the UFM image is the ripple features that occur with varying directions on the surface.

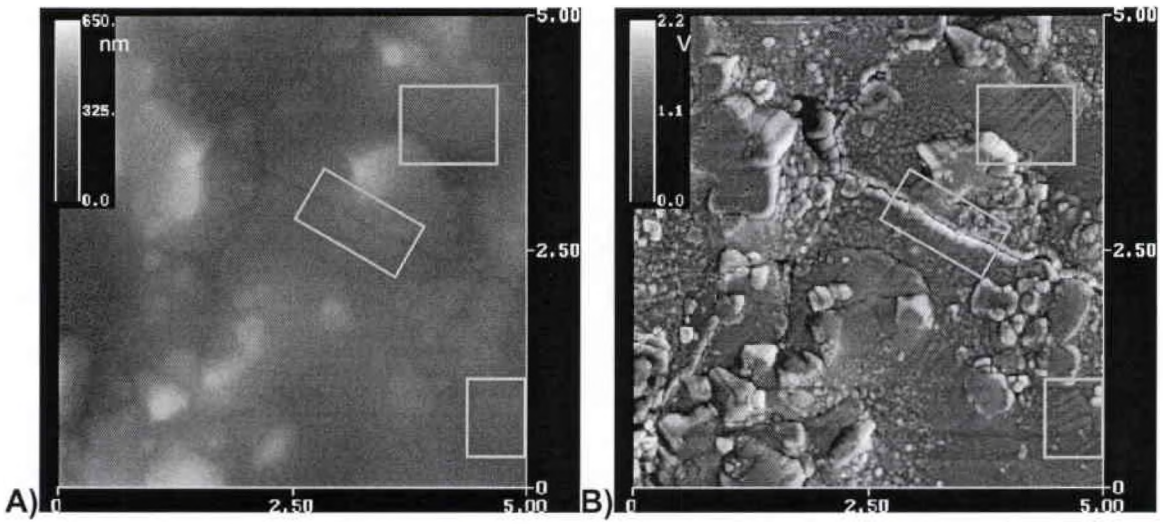

Figure 14: Slider #2 Exhibiting Material Changes From Loosened Grains, Surface Ripples Enclosed in the Boxes, and Nano Droplet Features
A) AFM surface topography image. B) UFM amplitude image
Imaged area is 5 μm x 5 μm.

It is thought that the rippled features occurred due to the very fast melting and solidifying that is occurring during the laser treated. The ripples seen on Slider#2 maybe an indication of the stress fields in the material.

AFM and UFM images obtained in the center region of Figure 14 at higher magnification are shown in Figure 15. At this very high magnification, the AFM image now starts to exhibit the presence of a crack among the changing topographic variation, though the overall contrast is fairly uniform. The UFM image (Fig. 15b) clearly exhibits the long main crack with its micro cracks branching from the side as well as the grain structure. The grains are observed with almost black to white contrast. Apart from the cracks and the grain structure, very small droplet-like-features that have diameters typically between 50-80 nanometers are also observed. In the upper right corner of Figure 15b is a region with a group of grains, which have separated from the entire matrix. One of the grains appears to be a twin rather than a single grain.

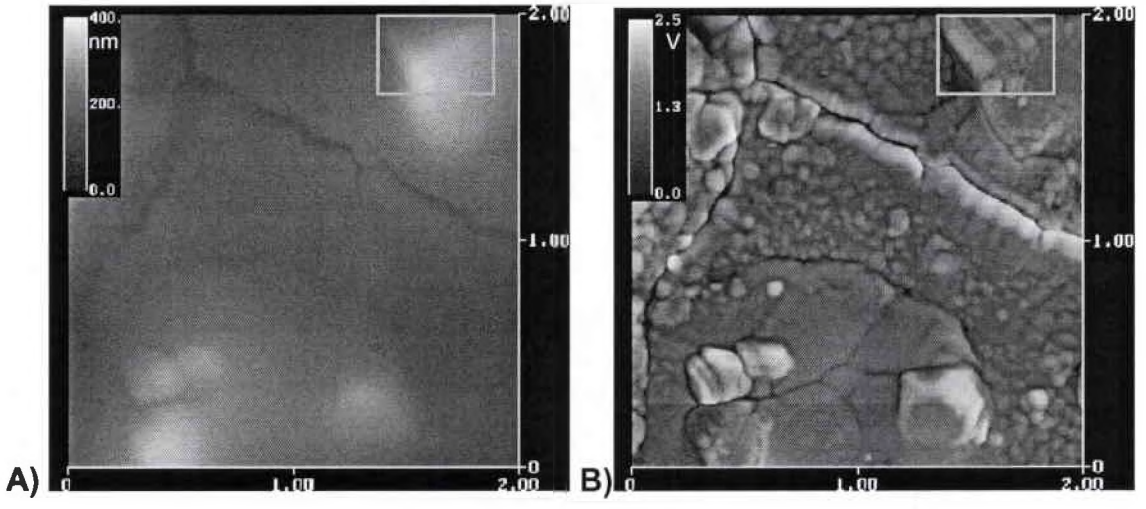

Figure 15: A Smaller Scan on Slider #2 Showing Possible Twinned Grain in the Highlighted Box, Scan area 2 μm x 2 μm

A) AFM surface topography image. B) UFM amplitude image

Figure 16 is a comparison of the amplitude variations along a line in the immediate vicinity of the crack for the same location on both the AFM and the UFM images. While the topography variations are fairly smooth (75 nm), the UFM scan exhibits rather large variations. This is especially clear in the rippled section along the crack between 1.2 μm and 2.0 μm of the line scan.

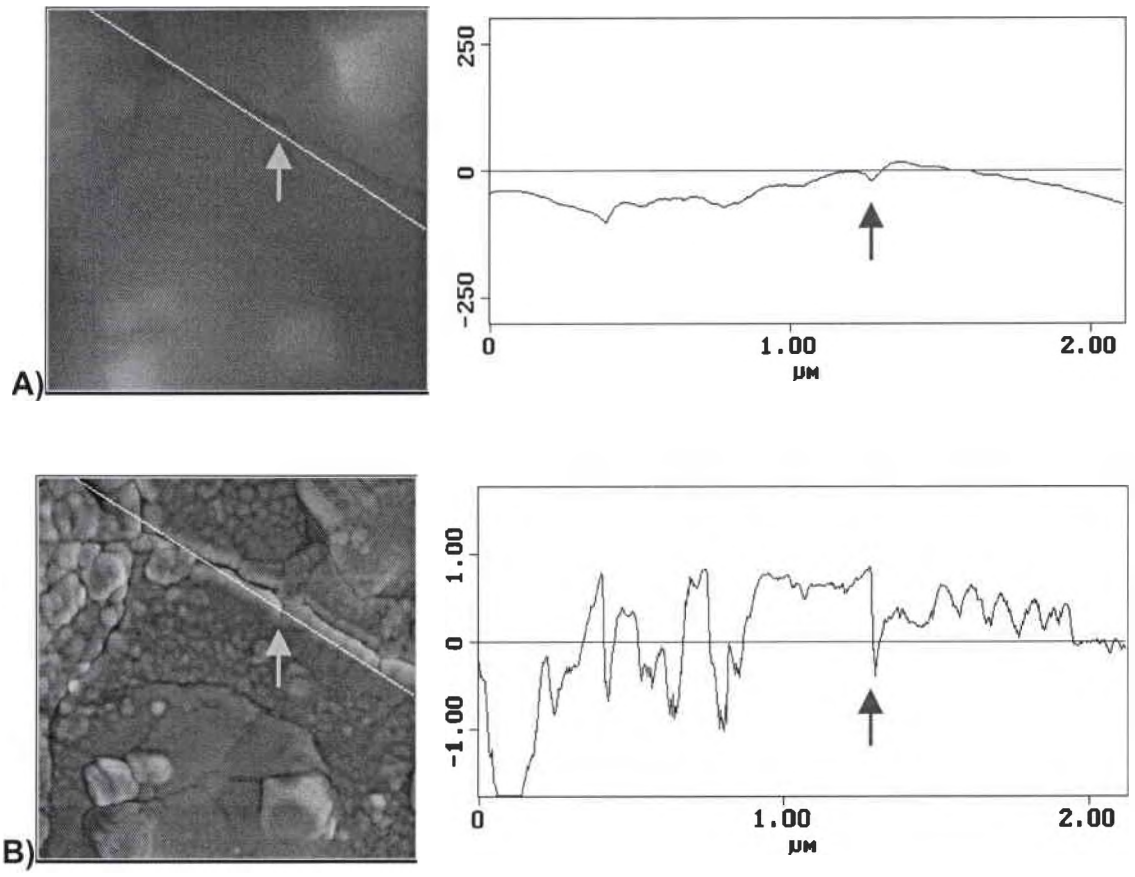

Figure 16: A Comparison of Identical Line Scans Across AFM and UFM Images The top line scan (A) is the AFM Topography while the bottom line scan (B) is UFM Amplitude with the images.

Figure 17 is a line scan from top to bottom on the same image while the main large crack in the top of the scan area can be detected in both images, the smaller cracks and loosened grains are only evident in the UFM analysis. The line analysis was selected in an area with little topography variation. Crack mouths that were opened more than 100nm could be imaged fairly well with the AFM but cracks smaller with an opening of less than 100nm could not be easily resolved.

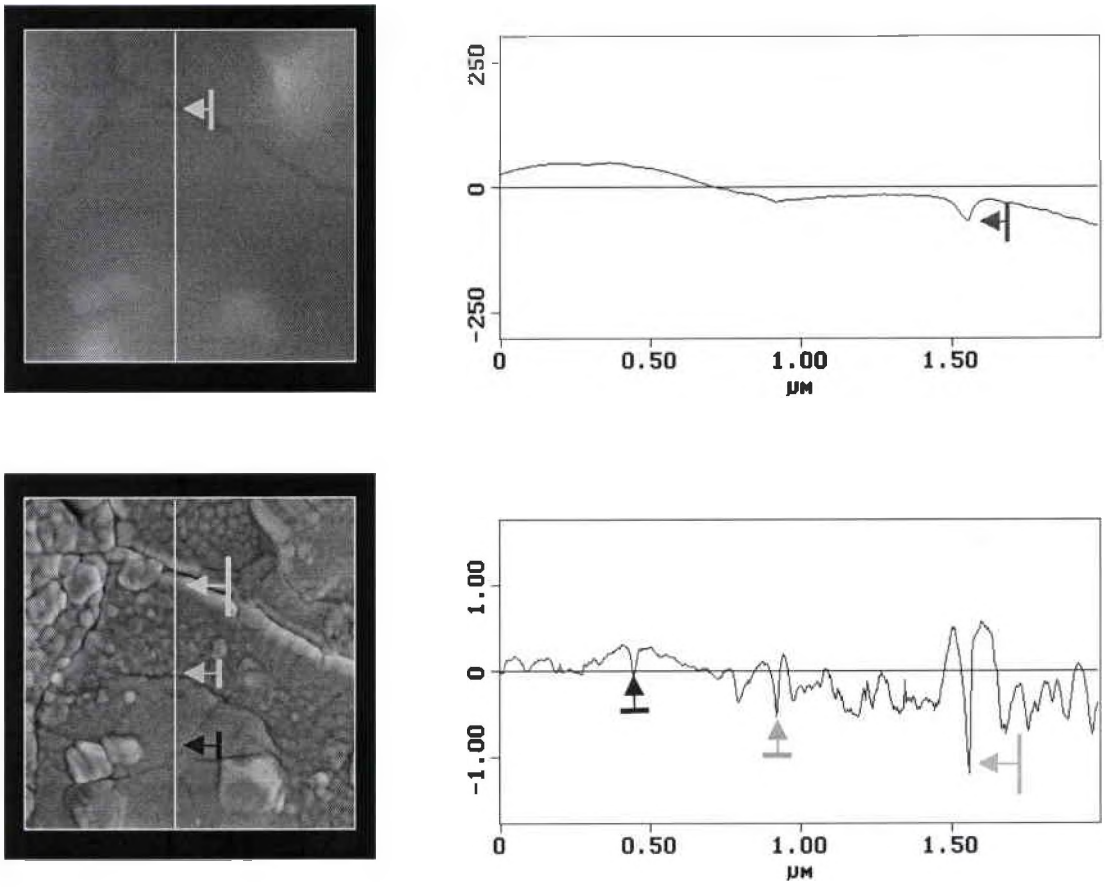

Figure 17: Vertical Comparison of Line Scans on AFM and UFM images
The top line scan is the AFM Topography while the bottom line scan is UFM Amplitude with the image indicating location of the line.

Unmodified Head Slider Surface

To compare the situation in the case of untreated sliders. AFM and UFM images were acquired on an unmodified surface. AFM and UFM images acquired in an untreated region on Slider #3 is shown in Figure 18.

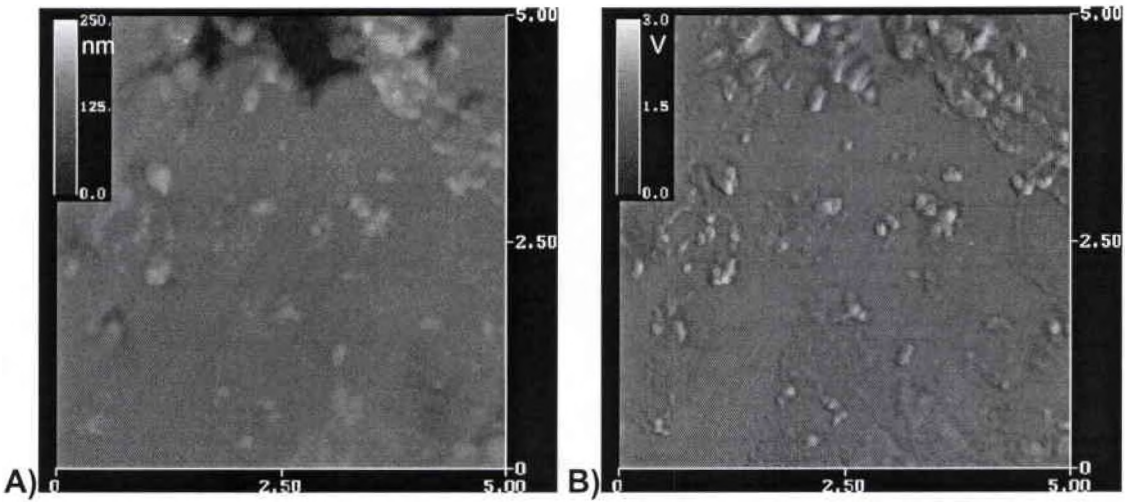

Figure 18: Untreated Surface Area on Head Slider #3
A) AFM surface topography image. B) UFM amplitude image @ 905 kHz.
Surface area scanned is 10 μm × 10 μm.

The AFM image shows topographic variations with a maximum height of 250 nm. The region in the top middle of the image show a feature indicating lower depth compared to the rest of the surface. The UFM image obtained at an ultrasonic frequency of 905 kHz shows almost all of the same features observed in AFM with better contrast. No cracking feature, indicating cracks were found in any of the images on the untreated slider.

2.6) Microcrack Discussion

In all of the slider images, it was observed that the contrast in the UFM images was much better than the surface topography images. It is well known that the contrast in the AFM images is due to the topographic variation [1]. On the other hand in the UFM scan, the tip interacts with the material underneath it as discussed in section 1.4. It is also believed that the depth sensitivity of the UFM is several times the diameter of the tip [9]. Hence the information contained in the UFM image is an averaged value from the top layers of the surface over a thickness of several times the tip diameter.

The ceramic head sliders are composites of Al_2O_3 and TiC. Al_2O_3 has hexagonal crystal structure and the elastic modulus varies with the crystallographic orientation. Since the material is polycrystalline the crystallographic orientation of each of the grains may not be similar. Hence the elastic modulus response of each of the grain is expected to be different. Thus even if the material surface is smooth and flat without topographic variations among several grains, the elastic modulus response can be different. Since UFM is sensitive to elastic property variations of the sample, the UFM image is expected to exhibit a better contrast than the conventional AFM image.

The hexagonal crystal structured single crystals of Al_2O_3 have two different thermal expansion coefficients, parallel and perpendicular to the basal plane. The two thermal expansion coefficients differ by about 10% at room

temperature. At higher temperature the differences between the A and C axis coefficient can become quite large as seen in Figure 19.

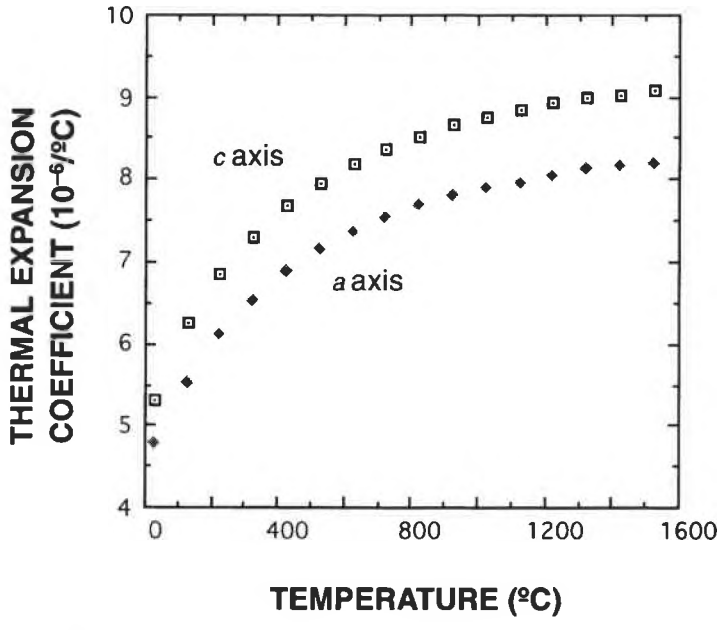

Figure 19: Thermal Expansion Coefficients of A & C Axis of Single Crystal Al_2O_3 [Green, D. J. "An introduction to the mechanical properties of ceramics," Cambridge University Press, New York, p. 96 (1998)]

When a polycrystalline Al_2O_3 material is heated uniformly, the adjacent grains expand differently. It is thought that the differential thermal expansion could generate large enough stress to induce cracking in the material [33]. While the sliders are undergoing laser treatment, the laser tooling can cause a dramatic increase in the temperature in localized regions. This rapid heating can lead to local variations in the thermal expansion in the Al_2O_3 grains. Further, upon cooling to room temperature tremendous thermal stresses can be induced causing cracking along the grain boundaries.

Besides a build up of stress between individual grains by the laser spot heating can be introduce a stress across a larger area of the sample. One can

use the flexural strength and elastic modulus to estimate the amount of strain that the entire material body can withstand. The strain and stress caused by the differential thermal expansion can be approximated using the equations.

$$\sigma = E\varepsilon \qquad \text{(Eqn-11)}$$

$$\varepsilon = \alpha_D \Delta T \qquad \text{(Eqn-12)}$$

where σ is the stress

E is Young's Modulus

ε is the strain

α_D is the maximum deviatoric component of the thermal expansion

ΔT is the change in temperature.

Using data from a manufacturer of Aluminum Oxide Titanium Carbide wafers, the raw material used in the construction of a head slider. The flexural strength, σ, is going to be a minimum of 550MPA in their material and the elastic modulus, E, is ~410GPA. Based on these number the material can withstand an estimated strain, ε, on the order of 0.0013.

The strain due to thermal expansion mismatch can be calculated using equation 12 for estimating the strain that would arise on rapid cooling of the ceramic material to room temperature. In the current case, the ΔT could be 1000°C or even 2000°C depending on the laser energy, repetition rate and scan pattern. The thermal expansion coefficient for Alumina and Titanium Carbide are listed in Table 2.

Material	System	α_{11}	α_{22}	α_{33}	Average
Al_2O_3	Hexagonal	8.1	8.1	8.8	8.3
TiC	Cubic	7.4	7.4	7.4	7.4

Table 2: Thermal Expansion Coefficient for Al_2O_3 and TiC [33]

Based on data for alumina with varying temperature intervals show that if the temperature at the center of the laser spot reached 2500˚C, thermal stress at the laser spot would crack the material.

$$\varepsilon = 0.5E\text{-}6\ (1000^{\circ}C) = 0.05\%$$

$$\varepsilon = 0.5E\text{-}6\ (2500^{\circ}C) = 0.13\%$$

The head slider composite contains up to 35% TiC. According one of the manufacturers of Al_2O_3-TiC that is used in head slider construction, the majority of TiC resides preferentially in the grain boundaries. The average thermal expansion difference between the Al_2O_3 and TiC is about 13% at room temperature. Assuming the temperature difference to be 1000˚C or 2000˚C, the thermal strain will be 0.09% or 0.18% These strains are significantly large compared to the thermal strains between alumina grains. This large thermal strain between the TiC and Al_2O_3 matrix might be one of the reasons for observing the long cracks running along the grain boundary.

In the laser treated region just in the immediate vicinity of the cracks, the ultrasonic displacement is much different from the rest of the matrix. One of the

possible reasons for the enhanced ultrasonic displacement is the free boundary condition along the crack flanks. A crack has a gap between its two flanks. The amplitude of the acoustic wave near the crack flank is expected to be larger due to the freeness of the boundary compared to the regions away from the flank of the crack. Because of the stress free boundary the ultrasonic displacement will be different than compared to other surface regions. This feature enhances the visibility of the crack. Due to the increased amplitude in the immediate vicinity of the cracks, the cracks in the UFM images appear brighter than the other regions. This enhanced amplitude helps in detecting the microcracks in the UFM. It is interesting to note that cracking is observed only inside the laser treated region and usually in the direction of laser treatment. In all the three sliders the laser-modified sections exhibit cracks while the untreated sections of the head slider do not exhibit any microcracking. All the cracks travel along the grain boundaries covering several grains.

In many regions, it appears that the shock of laser treatment may have loosened some of the grains from the surrounding material. Individual ~1 micron equiaxial grains of Al_2O_3-TiC can be distinguished in several of the UFM images. This grain structure appears very similar to the Al_2O_3-TiC grain structure which were seen on the ABS rails and in the starting raw material wafers that were studied and are discussed in Chapter 4. It should be noted that though the grain structure appeared similar in size, only in the laser treated region where larger ultrasonic signals detected at the grain's boundary region compared to the ABS section of the material.

A possible reason for the damage and the microcracking, is the thermal stress caused by the rapid increase in temperature and the rapid solidification. During the laser surface modification it is expected that the temperature increased beyond the melting point. Since the laser seems to be raster scanned during laser tooling repeated melting and cooling could lead to formation of tiny solidified droplets. These droplets might have a slightly different average elastic modulus compared to the rest of the matrix and hence are visible in the UFM images as spherical droplets of 50-80nm diameter.

Chapter 3 -Grain Size/Structure Analysis in Copper Microwires

3.1) Importance of Grain Size/Structure in Microwires

In the quest to build smaller and faster electronic devices, the microstructure of the microwires and interconnects is increasingly more crucial to the performance, reliability and lifetime of the device in a wide range of applications. With the development of smaller wires and interconnects in electronic devices, high resolution material characterization techniques need to be developed or refined, that meet the specific needs of the chip developers. Ensuring long term integrated circuit interconnect reliability has always been challenging because the failure of one individual interconnect out of the millions of submicron circuits can destroy the whole chip operation. A defect or crack needs only to be a mere 1micron in size to cause a catastrophic failure. Traditionally, the cause of interconnect failures were observed to occur after moisture exposure or temperature cycles so that chips were engineered to minimize these exposures [34]. The preference was to engineer in avoidance of conditions rather than to fully understand the fracture or failure mechanisms occurring.

The drive to shorten technology development cycles, shrink interconnect sizes and the adoption of new interconnect materials has lead to more

systematic studies. The increased importance of fracture and failure mechanisms and mechanics are leading the way. The interconnect material being employed is changing as developers switch from an aluminum alloys to copper in circuit wires. Copper allows for a finer wire width due to its lower resistivity than aluminum, a lower power consumption, better conductivity and electromigration resistance and hence is expected to improve the speed of the device [35-37]. Copper microwires can be made with a variety of grain sizes and textures based on the deposition method being employed during their fabrication. [38]

This has led to the development of techniques to produce optimized microstructure in copper wires. One of the techniques has been electrochemically deposited copper film (ECD). ECD copper films are now commonly used in high performance microelectronics. ECD copper films although produce optimized microstructures, can be unstable at room temperature due to the small grain size and the presence of atomic defects [39].

Characterization methods that further develop the understanding between the manufacturing processing conditions and the resulting microstructure are highly sought after because interconnect performance is strongly affected by both grain size and structure. Electromigration, precipitation formation, and grain stability are all influenced by both the deposited grain structure and by how the grain structure may be annealed or reformed during processing or end use operational heat cycles.

Diffusion processes, void growth and electromigration, play a large role in determining the reliability of interconnect structures in microelectronic devices.

Diffusional growth of voids in metal lines can cause resistance shifts in the interconnects that lead to failure. Voids are created by two primary mechanisms. One, by thermal stress due to the thermal expansion mismatch between the interconnect and the surrounding device material. The second mechanism is electron migration where atomic diffusion is caused by the momentum transfer from the conducting electrons. The motion of the atoms due to the electron flux can result in atoms piling up on one side of the metal line. This piling up of atoms can result in formation of a void, break or higher resistivity in the line.

While interconnects made from aluminum are isotropic and the stress mechanisms responsible for void formation are very well modeled and investigated over the last few decades. Interconnects made from copper which is highly anisotropic will discontinuities in the elastic modulus from grain to grain. The variations in the elastic modulus that can occur on crossing of grain boundaries, resulting in grain to grain variations in the stress state of the interconnect. Such effects may enhance void nucleation and growth when specific grain orientation or textures are present.

Another important aspect of void growth is understanding the pathways that aid in electromigration. Bulk diffusion is usually not the primary route. Parallel paths such as metal/metal grain boundaries and phase boundaries, and metal/device interfaces are thought to be more responsible. Therefore microstructure plays an important role in electromigration mechanisms. Despite more than 30 years of study the fundamental origin of this effect has still not been found.

Characterization techniques that can examine the grains in the device nondestructively over time or that have the ability to analyze the interconnects through a passivation layer, even if qualitative in nature, provides key feedback information to the device manufacturer [40].

3.2) Current Analysis Methods for Grain Structure

Some of the current characterization methods for studying the grain sizes and grain structures in microwires or interconnects are Transmission Electron Microscopy, Electron Back-Scattered Diffraction, Focused Ion Beam and X-ray. [41] Sample preparation and setup can be quite laborious, extensive and costly with these analysis methods. Furthermore imaging through a passivation layer may not be possible except in the case of high energy X-rays. [38]

The Atomic Force Microscopy has been applied to the study of deposition roughness and other topographical features during processing of copper thin films [36-37]. Some inferences on the interconnect material changes can be made from the AFM images topography although this is difficult and no clear connection to the underlying mechanisms can be assigned.

The adaptation of ultrasonics to the AFM allows a better insight in to the mechanical property changes that are occurring in the material, not necessary just on the surface. The UFM imaging of the elastic variations allows details of the microstructure, grain size, grain alignment, film morphology, defects or damage sites, along with time dependant changes to be brought forth in much greater detail.

3.3) Advantages of the AFM-UFM Method in Grain Structure Analysis

The UFM's qualitative elasticity image can be used to interpret the wire or interconnect's grain structure. It has been shown by previous work that the individual nanograins of copper can be clearly separated by this imaging technique without the need for chemical etching or extensive sample preparation [42]. In most grain structure analysis methods, the ability to analyze a wire's grain structure can become especially challenging and difficult without the aid of chemically etching the surface. But attempting to chemically etching submicron wires in a device may destroy the fine wires in the area of interest. Being able to image the grain structure in microwires, quickly and easily with minimal sample preparation, provides an additional tool that will speed device analysis, quality control and reliability checks for chip developers.

By using the contact stiffness variations (elasticity) across the sample, grains can be analyzed without the usual routine of chemical etching. With the UFM sensing the signal coming through the sample and detecting material changes subsurface, the possibility arises of imaging the grains in a wire under an overcoat layer. The possibility of having a material testing technique that can evaluate the grain structure nondestructively after an electrical device has been in service will allow new ways to do time dependant studies of the grain size/structure changes. By being able to watch the grain structure evolve during the device life has the potential to aid in the understanding of electrochemical

migration, void formation and growth, and environmental failure mechanisms. Maintaining the preferred stable grain structure in the microwire during its lifetime is also important in regards to having the device operate at its peak efficiency [18, 41].

3.4) Copper Microwire Materials

Copper microwires of various widths, from 400-2000 nanometers, usage (aged) state and at different stress locations in the device have been examined using the AFM-UFM technique. In this characterization, the copper microwires were positioned on top of a 1 mm thick substrate base. The copper deposition process used to create these samples and their exact location in the device will not be discussed. The application of the AFM-UFM for material characterization and imaging for the study of copper wire grains will be presented. Samples were analyzed at a scan rate of 0.3-0.8 Hz with the ultrasonic frequency usually between 700-905kHz. V-shaped silicon nitride probe tips with a spring constant of 0.12 were used for the measurements.

3.5) Result For Copper Microwire

Bare Copper Microwires in a Device

Device samples with different width thin film copper microwires were evaluated. The wires are manufactured with a coating over them to protect and preserve the wires. For the initial study, the protective layer above the wire was removed by a mechanical means. The coating was removed to ensure an unblocked signal from the copper wire and to mediate any overcoat signal issues in the initial study. The following is an overview of the material characterization and images that were recorded on the device wires.

Figure 20 is an image on a 1.5 μm wide section of wire that was obtained at an ultrasonic frequency of 776 kHz. The surface topography height scale is 0-350 nm with most features being below 200 nm in height. Inadvertent hitting of the sample during a positioning adjustment caused the high spot (debris) visible in the lower left quadrant of the image.

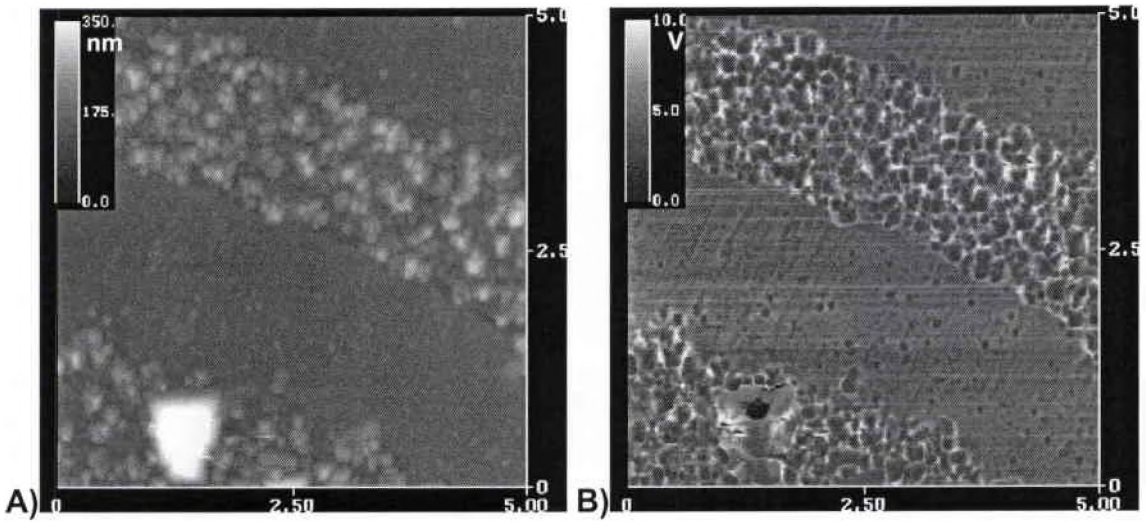

Figure 20: A Microstructure Image of Copper Grains in 2 µm Wires
A) AFM Surface Topography Image. B) UFM Amplitude Image. Imaged area is 5 µm x 5 µm.

The AFM topography image allows some inference of the individual grains in the wire but the UFM image clearly has a better level of detail and contrast. Figure 21 is a smaller scan area acquired at the same frequency, higher magnification image that emphasizes the clarity of the grain imaging.

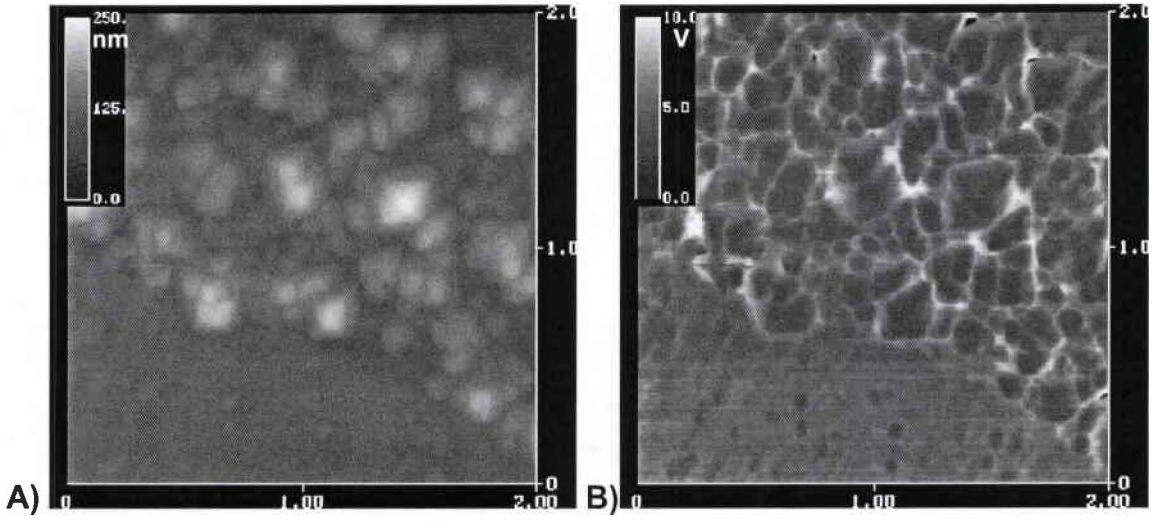

Figure 21: Higher Magnification of the Wires in Figure 19
A) AFM Surface Topography Image. B) UFM Amplitude Image. Imaged area is 2 µm x 2 µm.

To perform a quantitative analysis of the grain size distribution from an AFM image can be very difficult. Even with the aid of offline computer image enhancement, using the AFM topography information for grain sizing is very difficult. On the other hand, the UFM image of the same region displays the details of individual grain structure and makes discerning grains easier. The enhanced contrast is due to elastic anisotropy of the wire material. The UFM image was used to determine an average grain size in that section of wire. Using a simple analysis on the UFM image, an average grain size was calculated and determined to be 150 nm. The sizing method consists of counting the respective individual grains and dividing the total numbers of counted grains by the area of that section of wire while assuming a circular structure to the grains. The grain size measurements were performed offline using Image Pro Plus software.

Another sample showed a similar grain structure to the wire seen in Figures 20 and 21. Figure 22 is an image on a 2 μm wide wire segment from a different sample acquired at a frequency of 820kHz. The grain size was analyzed in a similar fashion to the prior sample; also assuming a circular grain structure, its average grain size is 430 nm or roughly 3 times as large. Most of the surface height features in Figure 22 are less than 100 nm tall. Figure 23 explains the counting and grain diameter determination.

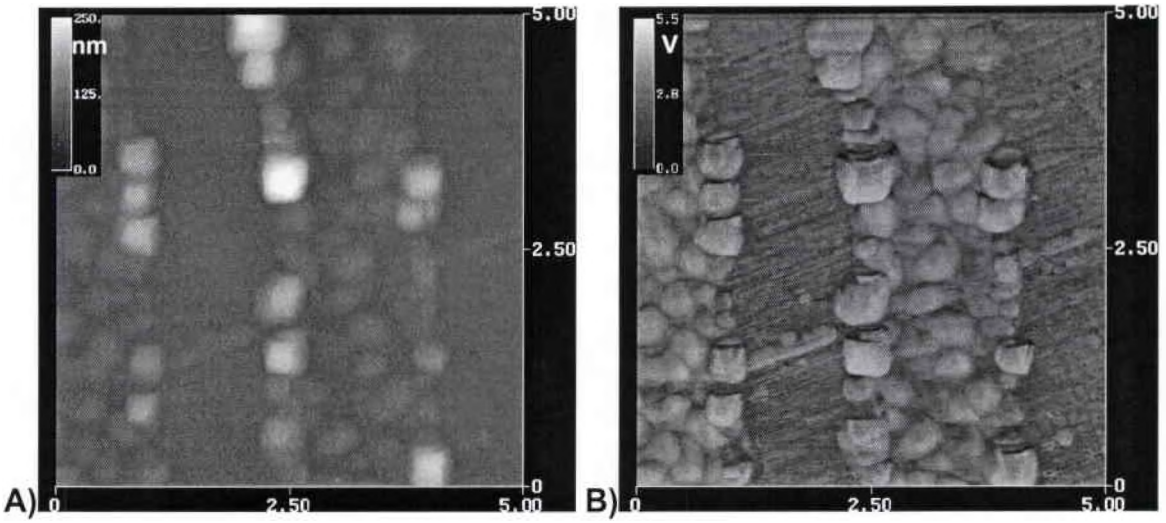

Figure 22: Microstructure In a 2 µm Width in Service Wire

A) AFM Surface Topography Image. B) UFM Amplitude Image. Imaged area is 5 µm x 5 µm.

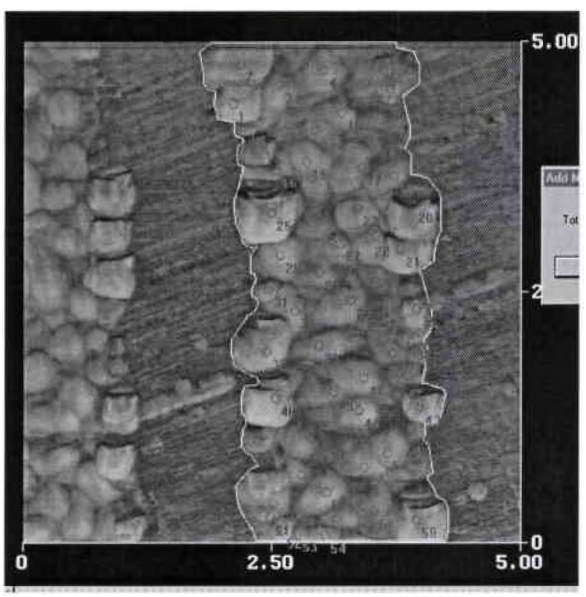

Figure 23: Image Detailing Area and Grain Count Calculations

Figure 22 is on a microwire from a used (in service) device whereas the microwires in Figures 20 and 21 were from a device that had not been in service.

The larger grain structure could be the result of annealing or restructuring from the heat generation during usage. It could also be caused by precipitate formation and grain growth as a result of electronic migration or environmental effects.

The environmental effects may have resulted after the protective coating was removed and before the wire was analyzed. Since the protective layer was removed at another location, a time delay was often incurred before the wire was imaged. The wires did corrode if an attempt was made to clean them off with any liquid media, though cleaning was rarely needed and usually the devices were imaged as is, with no further sample preparation. Over time especially if the samples were wetted with any solvent, rapid deterioration of the wire occurred. All imaging was done on the sample before they exhibited any visible environmental exposure effects. All sample images shown were done on devices that did not exhibit visible signs of wire deterioration before analysis. Figure 20-22 demonstrates the power of the UFM technique for studying microstructural changes occurring over time in microelectronics devices due to usage.

Sub-micron width wires were also subjected to the same imaging technique. Figure 24 shows several half micron wide microwires with Figure 25 shows a closer examination of the second wire from the right in Figure 24. Both Figure 24 and Figure 25 were collected at an ultrasonic frequency of 862 kHz.

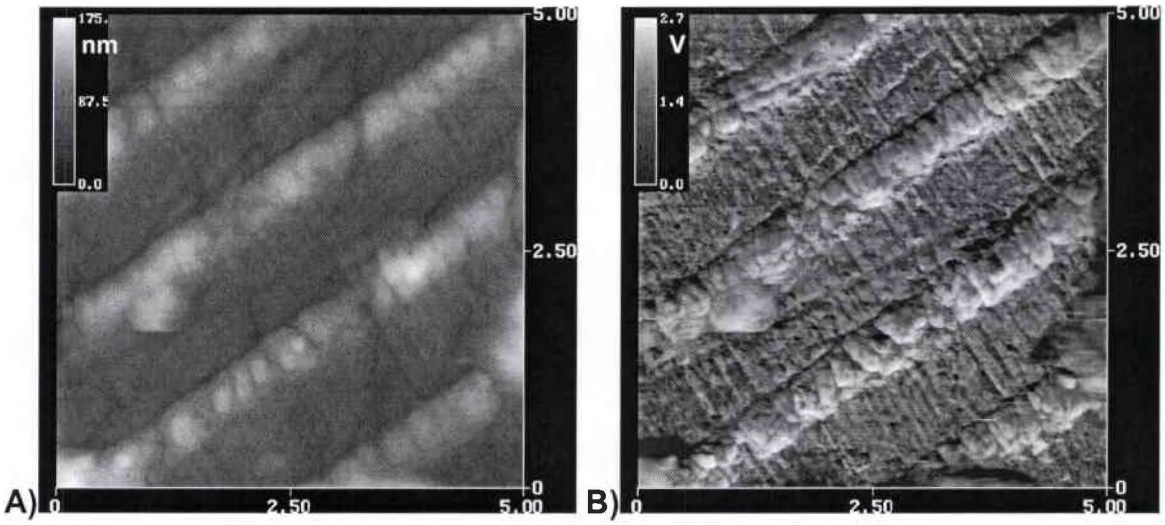

Figure 24: Microstructure of 0.5 µm Wide Microwires
A) AFM Surface Topography Image. B) UFM Amplitude Image
Imaged area is 5 µm x 5 µm

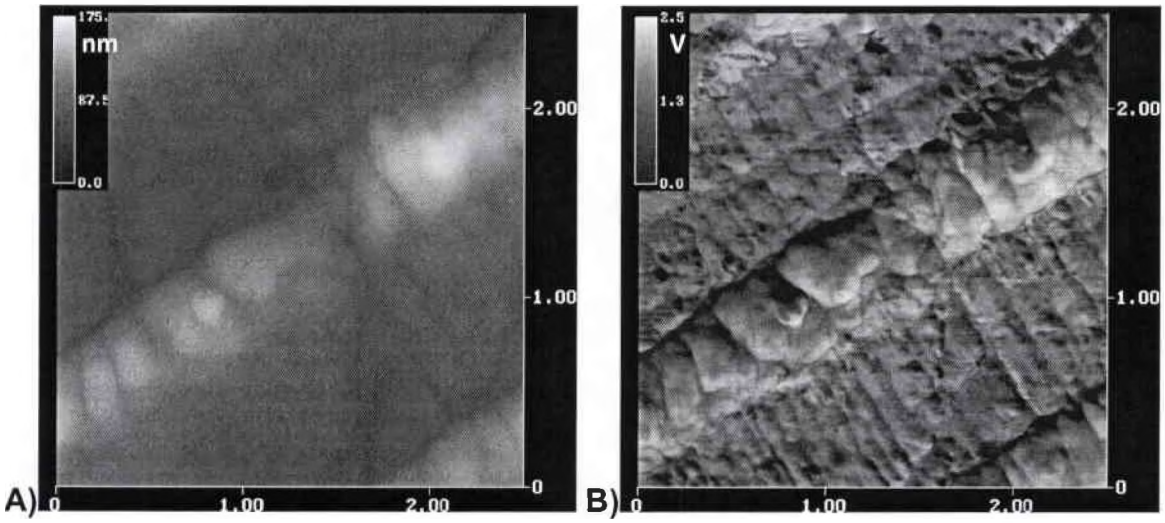

Figure 25: Higher Magnification of Single Wire from Figure 24
A) AFM Surface Topography Image. B) UFM Amplitude Image
Imaged area is 2.5 µm x 2.5 µm.

In the 500 nm wide wires, each individual copper grain appears to have developed to the width of the entire wire. The individual grains encompass the

entire wire width and the wire has a single line of grains running its length. This structure appears similar to the bamboo grain structure that is preferred in order to minimize electromigration. The bamboo structure has been found to develop or occur after annealing [41,43]. The grain size in these wires is roughly 300 nm. During device operation, the finer wires could bear the burden of a higher heat exposure and reach a higher temperature than wider width wires. The higher temperature in thinner sections of wire may have resulted in the material annealing. Annealing could be the cause of the different grain structure. This is especially possible since it was believed that the grains in this narrow wire section were larger than at initial deposition and secondly the section of thinner wire diameter has larger grain sizes than a connecting wider section of the same wire.

Another important area of research that the AFM-UFM technique can provide feedback on, is in quality and reliability inspection of the fine wires for discrete breaks or microstructural changes in the wire due to usage over time. With device minimization, the finer wires can be subjected to localized heating leading to annealing and grain size changes that will affect the resistivity of the wire. Figure 26 is an image of another sample's 500 nm wide wires acquired at 805kHz. The surface topography is fairly flat (less than 100 nm) and the AFM image lacks the fine wire details. The contact stiffness map in the UFM image allows for the wire structure to be seen in greater detail and for a vastly improved view of defects or breaks.

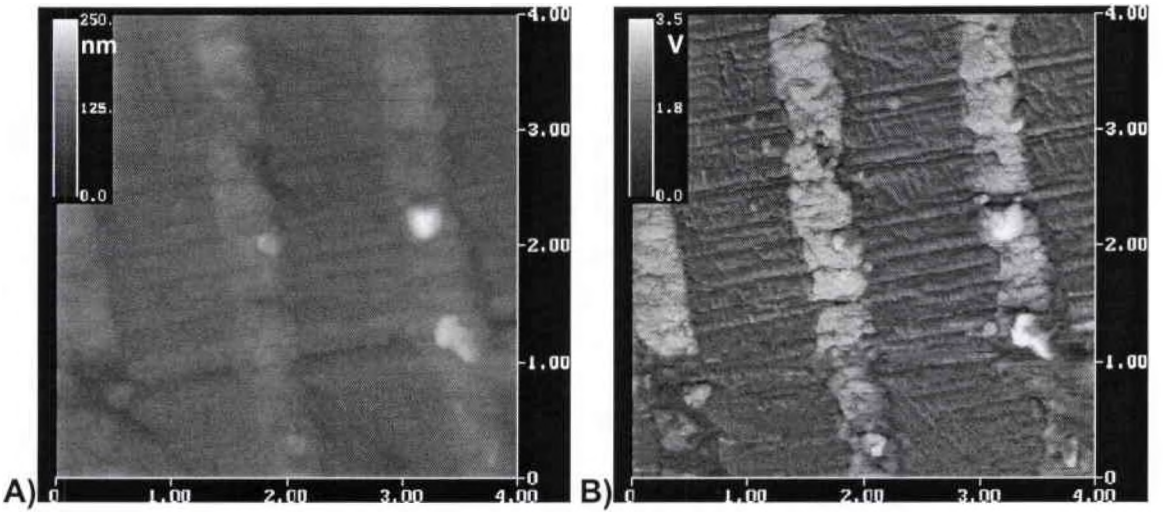

Figure 26: Microstructure in 2nd Set of 0.5 µm Wires
A) AFM Surface Topography Image. B) UFM Amplitude Image.
Imaged area is 5 µm x 5 µm

Learning more about the void morphology is important in trying to link the mechanisms to the cause for electromigration failure in copper [36-37]. These same studies also indicate a relation between the lifetime of a wire and its grain size [36-37].

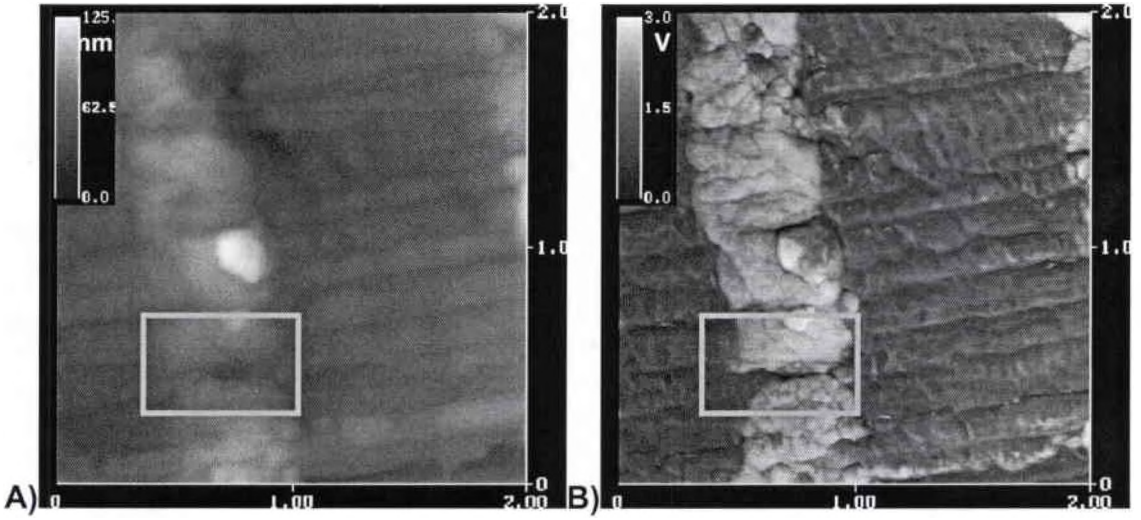

Figure 27: Highlighting Break Feature from a Line in Figure 25
A) AFM Surface Topography Image. B) UFM Amplitude Image
Imaged area is 2 µm x 2 µm

The highlighted box in Figure 27 shows what appears to be a fine break in the middle wire on Figure 26. The break does not appear to have been caused during the mechanical removal of the overcoat based on the lack of surrounding wire damage that would suggest polishing was the cause of the break. In the AFM image, it is hard to discern if the highlighted box contains only a void with some of the wire still connected. The UFM's elasticity image allows a nanometer fine break to be resolved. The ability to detect fine changes and breaks in microwires and interconnects can allow scientists and engineers to quickly locate the exact failure spot in the device. The ability to obtain high resolution images of these break structures and the device status is very valuable information. A knowledge of the exact location of a device failure initiation will in turn aid in understanding the failure mechanisms and hence speed development of a design solution.

Method Evaluation of Coated Copper Thin Film

A preliminary extension of the microwire study was to determine the general feasibility of using the UFM to image copper grains with a protective coating in place. The device microwires imaged previously had a thick coating over the wires that was removed prior to imaging since the coating was much thicker than the subsurface sensing ability of the UFM. Test samples were manufactured where a thin film copper layer was deposited on a silicon wafer with a very thin protective oxide layer over the top of the copper. A series of images taken on the sample are shown in Figures 29-34. The AFM topography images show minor details of the grain where as the UFM appears to highlight more substantially the entire grain and the grain boundary region.

Figure 28 was acquired at a frequency of 885kHz on the copper thin film. Discerning the grain structure is not easy at the 10 micron imaging scale.

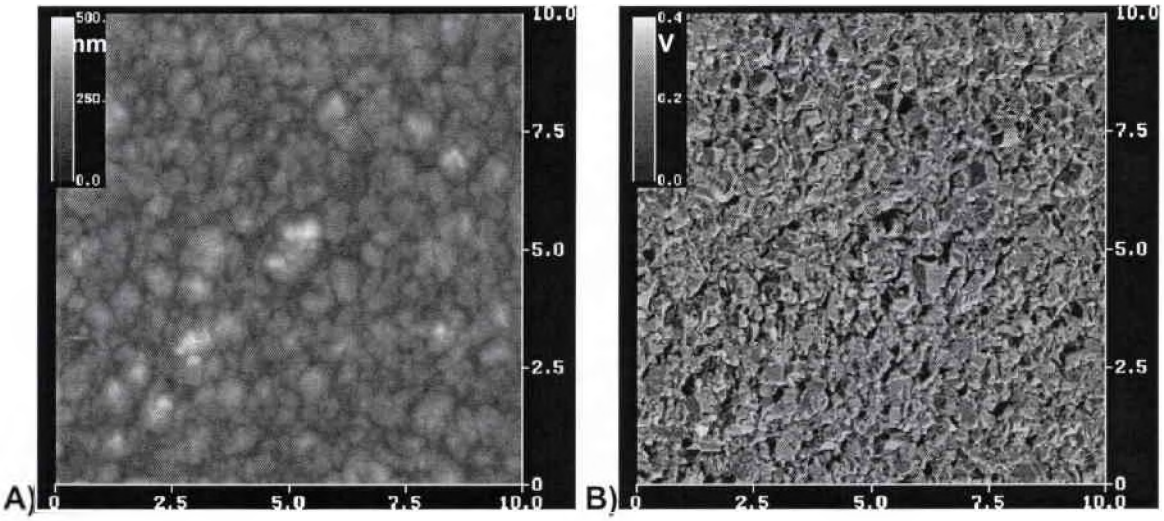

Figure 28: Coated Copper Thin Film
A) AFM Surface Topography Image. B) UFM Amplitude Image.
Imaged area is 10 μm x 10 μm

The higher magnification image at 5 micron and at the same excitation frequency starts to show more of the grain structure details. It should be mentioned that when the copper was deposited it was hoped the thin film could be grown with minimal surface topography. This was not the case as the surface height variations were typically in the range of 300 –600 nanometers across the surface.

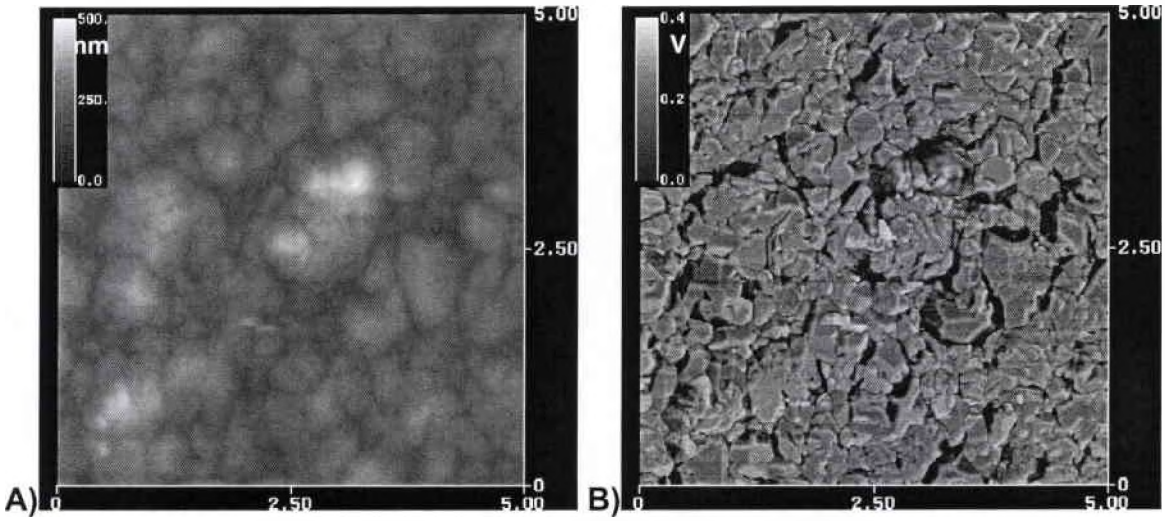

Figure 29: Copper Thin Film Structure at 5 µm
A) AFM Surface Topography Image. B) UFM Amplitude Image.
Imaged area is 5 µm x 5 µm

Figure 30 is a 2 micron image acquired at an ultrasonic frequency of 885kHz. There is a good contrast at what appears to be grain boundaries. It appears the elasticity variations between grains and the grain boundary is beginning to be sensed by the UFM.

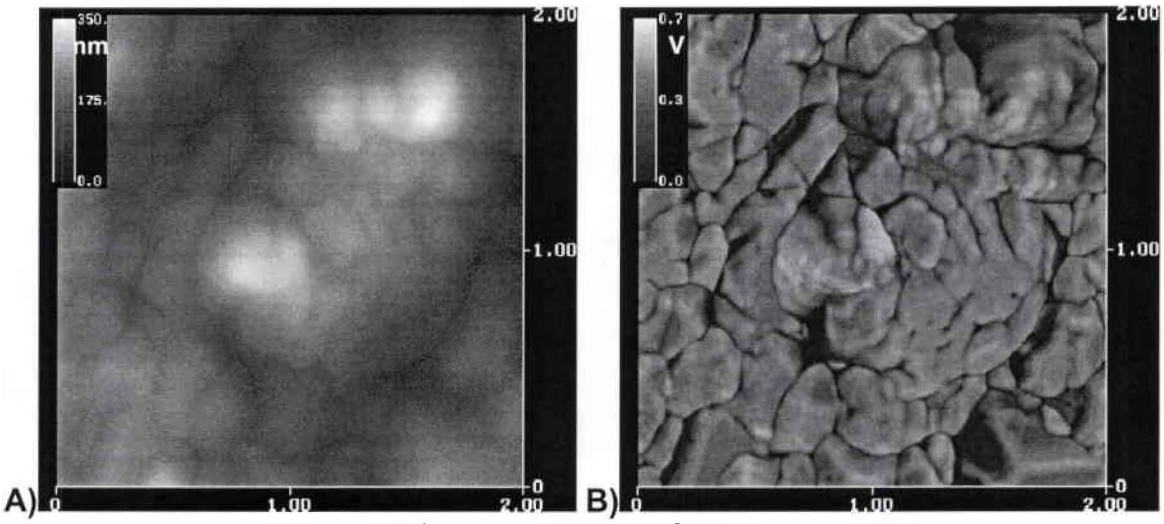

Figure 30: Copper Thin Film Structure at 2 μm

A) AFM Surface Topography Image. B) UFM Amplitude Image.

Imaged area is 2 μm x 2 μm

Images acquired on other areas of the copper thin film showed similar features as those seen in Figure 28-30. Imaging at different ultrasonic frequency did not appear to change the features detected in the AFM or UFM. Figures 31 and Figure 32 were acquired at lower frequencies of 411kHz and 526kHz respectively. Figure 30 is the best example of where the UFM could aid in detecting the grain size of the particles.

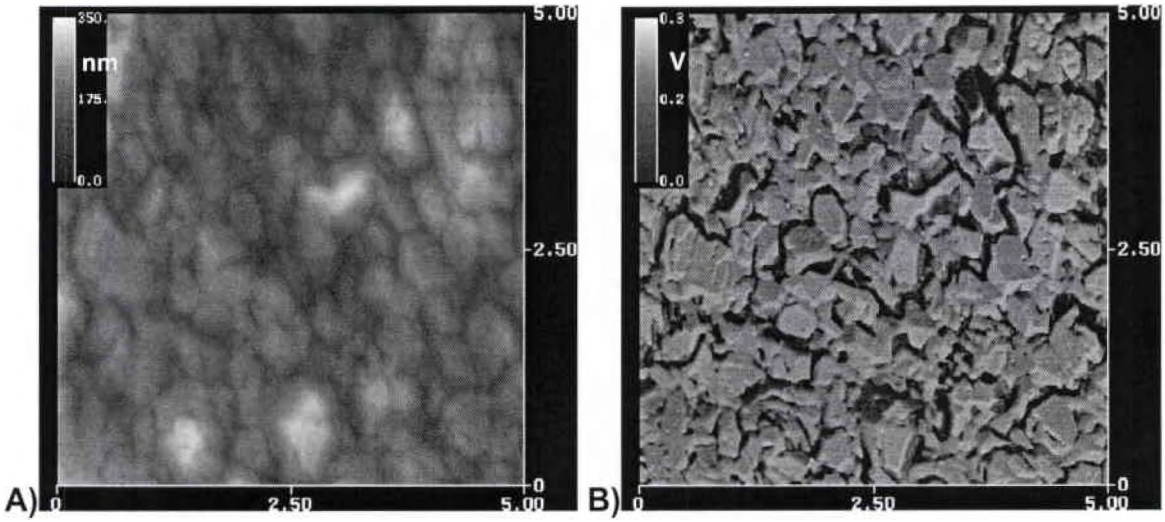

Figure 31: Copper Thin Film Structure at Lower Frequency 1
A) AFM Surface Topography Image. B) UFM Amplitude Image.
Imaged area is 5 µm x 5 µm

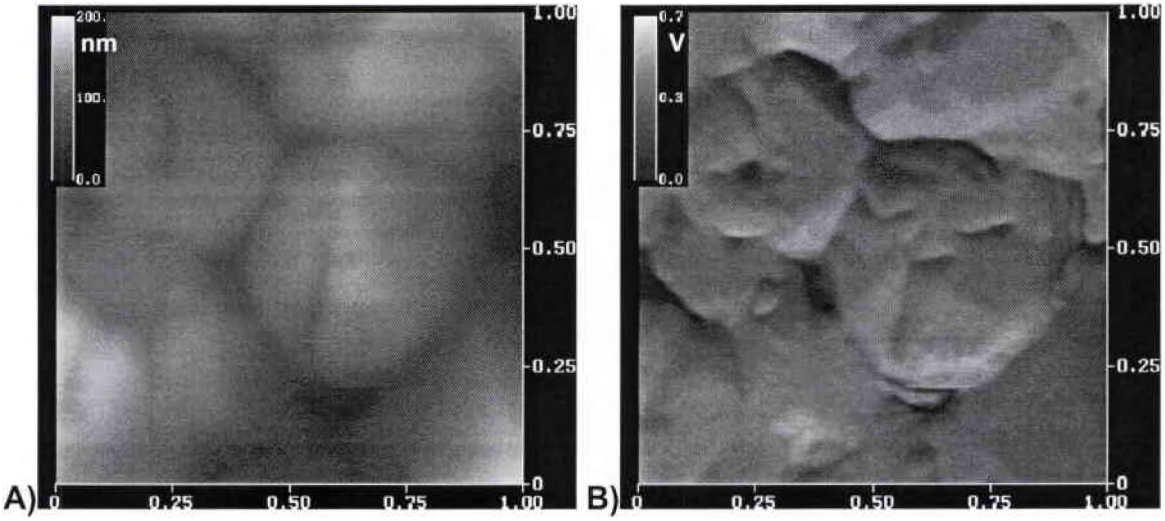

Figure 32: Copper Thin Film Structure at Lower Frequency 2
A) AFM Surface Topography Image. B) UFM Amplitude Image.
Imaged area is 1 µm x 1 µm

Attempts were made to remove the protective overlay and leave the copper layer relative intact in order to attempt to verify the copper grain structure. It was felt that chemical etching would remove both the overcoat and the copper

layer or degrade the copper layer. To overcome these problems with chemical etching, thermal etching was attempted. Images taken across the thermally etched samples showed that the sample appeared to be still coated in some areas. Figure 33 shows a 3 micron scan on the etched sample acquired at 886kHz.

The sample appears to have been heated to the point that grain nucleation and growth were initiated. Though the underlining major features of the grain appear very similar to the non thermal etched images.

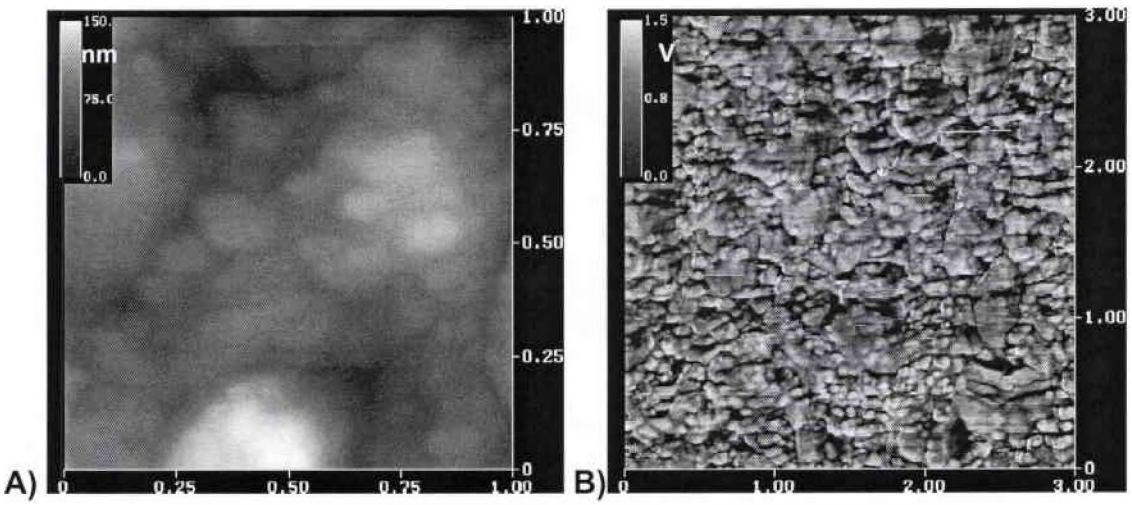

Figure 33: Thermal Etched Copper Thin Film Sample
A) AFM Surface Topography Image. B) UFM Amplitude Image.
Imaged area is 3 μm x 3 μm

Figure 34 is a higher magnification image of the same area at the same frequency as Figure 33. The suspected grain growth features appear very clear in the higher magnification scan. The smaller particulate seen in Figure 33 is believed to be new grains developing. Both figures were acquired at 886kHz.

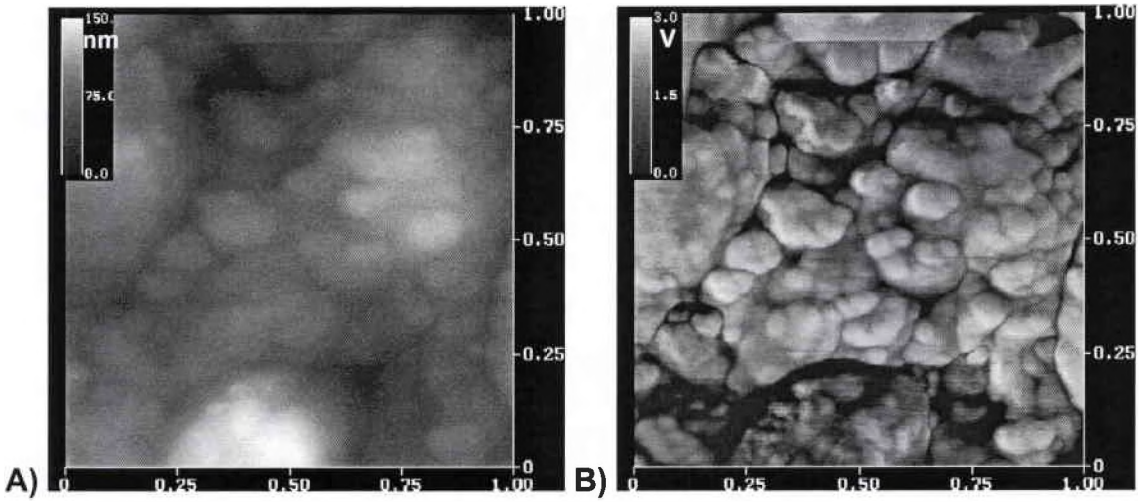

Figure 34: Higher Magnification on Thermal Etched Copper Sample
A) AFM Surface Topography Image. B) UFM Amplitude Image.
Imaged area is 1 µm x 1 µm

The appearance of crystal formations on other sections of the etched coated sample led to this conclusion that the coating had not been fully removed in all sections, Figures 35-36 are images of the crystal formation seen on the sample surface. Figures 35-36 were acquired at 758kHz. The topography in this section of the sample was much greater. With the tallest crystals extending almost 2 microns from the surface.

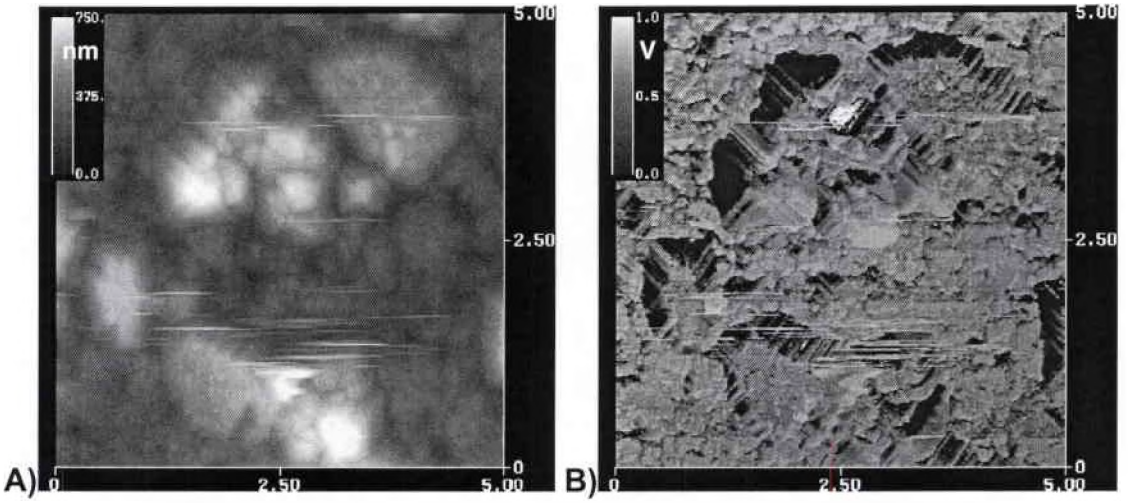

Figure 35: Thermal Etched Sample with Coating Remaining
A) AFM Surface Topography Image. B) UFM Amplitude Image.
Imaged area is 1 µm x 1 µm

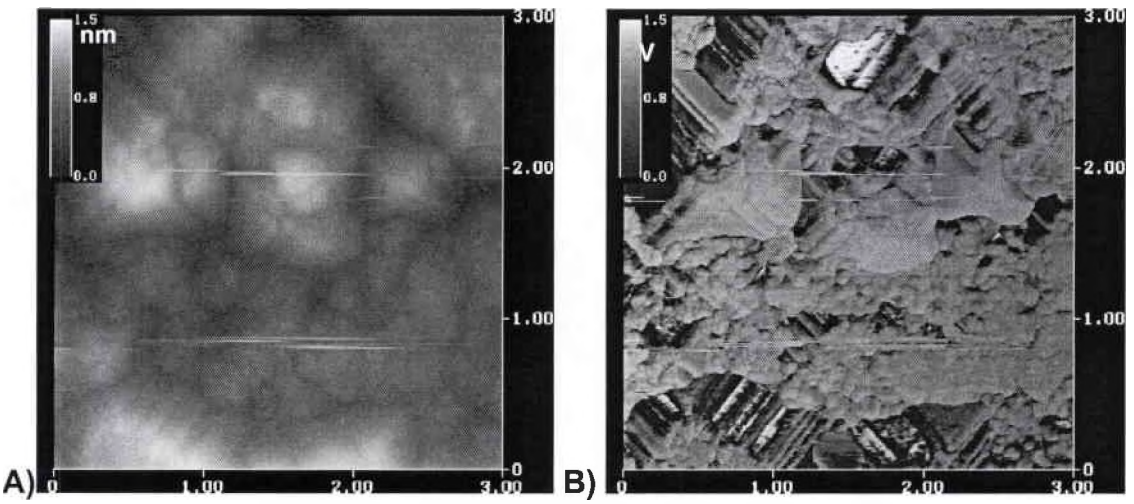

Figure 36: Higher Magnification of Figure 34
A) AFM Surface Topography Image. B) UFM Amplitude Image.
Imaged area is 1 µm x 1 µm

One, hindrance on the test wafer investigation was the fact that the copper film was not planned flat before the overcoat was applied. As a result, surface height variations up to 2000nm were observed, although most areas were ~500-700nm. Without removal of the height variations, a firm conclusion on the subsurface

analysis of copper can not be obtained. The preliminary results did indicate a strong possibility that the UFM is capable of imaging the copper grain through a very thin coating. The UFM contact stiffness measurement extends subsurface into the material to a depth of 3-10 tip diameters. If the tip radius is 15nm, then the coating thickness needs to be less than 50-150 nm for the UFM to be able to image through it.

3.6) Copper Microwire Discussion

In all of the image comparisons, the UFM allowed for a more detailed image of the grain structure than was possible by conventional AFM. In the AFM images, the image contrast is the result of the topographical changes in the sample surface. In the UFM the probe tip interacts with the material below the tip extending to a few atomic layers below the surface. Copper is elastically an anistropic material and so the changes in modulus for different orientations are quite large which aid in the system's imaging ability.

Copper has a face centered cubic crystal structure. The elastic constants for cubic copper are C_{11}=16.84, C_{12}=12.14 and C_{44}=7.54 (units dyn/cm^2 x10^{-11}) [44]. C_{11} is a compressional longitudinal wave and the other constants C_{12} and C_{44} are transverse shear waves. A measure of the anisotropy in cubic crystals is the ratio of the two shear moduli that is given by Zener ratio or the elastic anisotropy factor [33].

$$Z = 2C_{44}/(C_{11}-C_{12}) \qquad \text{(Eqn-13)}$$

The Zener ratio for copper is 3.21 which is an indication that copper is highly anistropic. A Zener ratio of 1 would indicate an isotropic material such as aluminum, which has a Zener ratio of 1.28. The different crystallography directions in the copper material will exhibit difference in contrast. It had been shown in a study of polycrystalline copper that the grain structure could be

observed by acoustic microscopy and that the contrast was attributed to the large elastic anisotropy of copper [45].

While the microwires are polycrystalline, during manufacturing great car is taken to have only one preferred orientation direction. Depending on the application and operating environment either <110> or <111> may be present. Since all of the grains are deposited and grown with an aligned crystal direction, the UFM will not exhibit the grain to grain variation seen in prior work by Schumaker et al [42]

On the copper microwire images, the grain to grain contrast is fairly even. The grain to grain contrast should be even if the tip is imaging on the same crystallographic direction. But the grain boundary region between two grain exhibits a much different contrast. One can think of the grain boundary region as the tie down or connection point between the grains. Though the grain bodies are exhibiting similar responses, the grain boundary is confined in keeping the grains to the matrix or its acting as an interaction plane between the two neighboring grains and so is exhibiting a different contrast.

The AFM-UFM technique allowed the grain structure to be examined in these fine wires. By examination of devices that have been subjected to different workloads and conditions, this method may allow for a better understanding of the mechanisms that initiate grain changes, void growth or electromigration in the wires.

Chapter 4 -Investigation of Grain Boundary Inhomogeneities

4.1) Applications for Al_2O_3-TiC Wafers

Aluminum Oxide-Titanium Carbide, Al_2O_3-TiC, composite wafers are micro-engineered for use in the thin film head and modern hard disc drive industry. This ceramic is used in the construction of Nano, Pico and Femto format heads and is also used in microelectronic applications where the conductivity of the Al_2O_3-TiC material allows safe elimination of static build in applications such as magnetic recording [46]. In slider construction, Al_2O_3-TiC is employed for its wear and durability properties and also its ability for machine lapping with minimal chipping or cracking in the machined surface [18].

4.2) Grain Pullout Issues

An ideal wafer will have a pore-free homogeneous microstructure and be resistant to grain pullout and particle shedding during mechanical polishing or application use. A poor wafer will allow single grains to pull loose from the polished surface thereby creating problems and defects in the final product. A technique is needed that can evaluate the grain boundary region between grains. One of the possible causes of grain pull out is a lack of strong grain bonding to the surrounding grains through the material in the boundary region. A non-

uniform distribution of the binding material in the grain boundary could cause defects in local regions that allow loosening of the grains to occur.

4.3) AFM-UFM for Grain Boundary Analysis

The purpose of the investigation has been to test the feasibility of the AFM-UFM method as a quality control technique for evaluation of Aluminum Oxide-Titanium Carbide ceramic composite wafers. The AFM posses the nanoscale resolution ability to investigate the extremely small grain boundary region. The addition of UFM would allow a measurement of elastic modulus variations in the grain boundary area. This incorporation of the elastic inhomogeneities into the image should allow a better observation of every grain as well as the grain boundaries in great detail, which can't be seen in conventional AFM measurements.

4.4) Aluminum Oxide Titanium Carbide Wafer Materials

The wafers were manufactured by hot isostatically pressing (HIP) process. The samples were prepared with a series of polishing steps culminating in a final polish with a 0.05-micron diamond paste. All of the wafer samples were subjected to the same polishing routine to ensure that the samples were maintained at the same base condition for analysis. The Al_2O_3-TiC ceramic composite wafer samples had dimensions of 11 mm x 11mm with a thickness of

2 mm. The approximate composition of the wafers were approximately 65%-69% Al_2O_3, 29-33.5%TiC with the remaining percentage being binder, additives or alloying elements. The exact material composition is highly propriety and was not released.

4.5) Al_2O_3-TiC Grain Boundary Results and Discussion

Al_2O_3-TiC Substrate Wafer Results

AFM-UFM images were acquired on all of the samples as described in Chapter 1. Four different wafer lots were evaluated in order to observe how the grain structure and grain boundary region was affected. Since the emphasis was on the observation of uneven contrast distribution along the grain boundaries, images with a larger (10μm x 10 μm) area were acquired. This was done so that more grain boundary regions could be covered with a reasonable level of detail. The larger area, covering 20 or so grains, allowed groups of grains to be compared relative to one another. One of the first observations made among the examined Al_2O_3-TiC wafer samples is that the grain sizes as well as the grain shapes were different. Figure 37 shows images taken on sample lot #1 and sample lot #5. Both images were acquired at an excitation frequency of 730kHz.

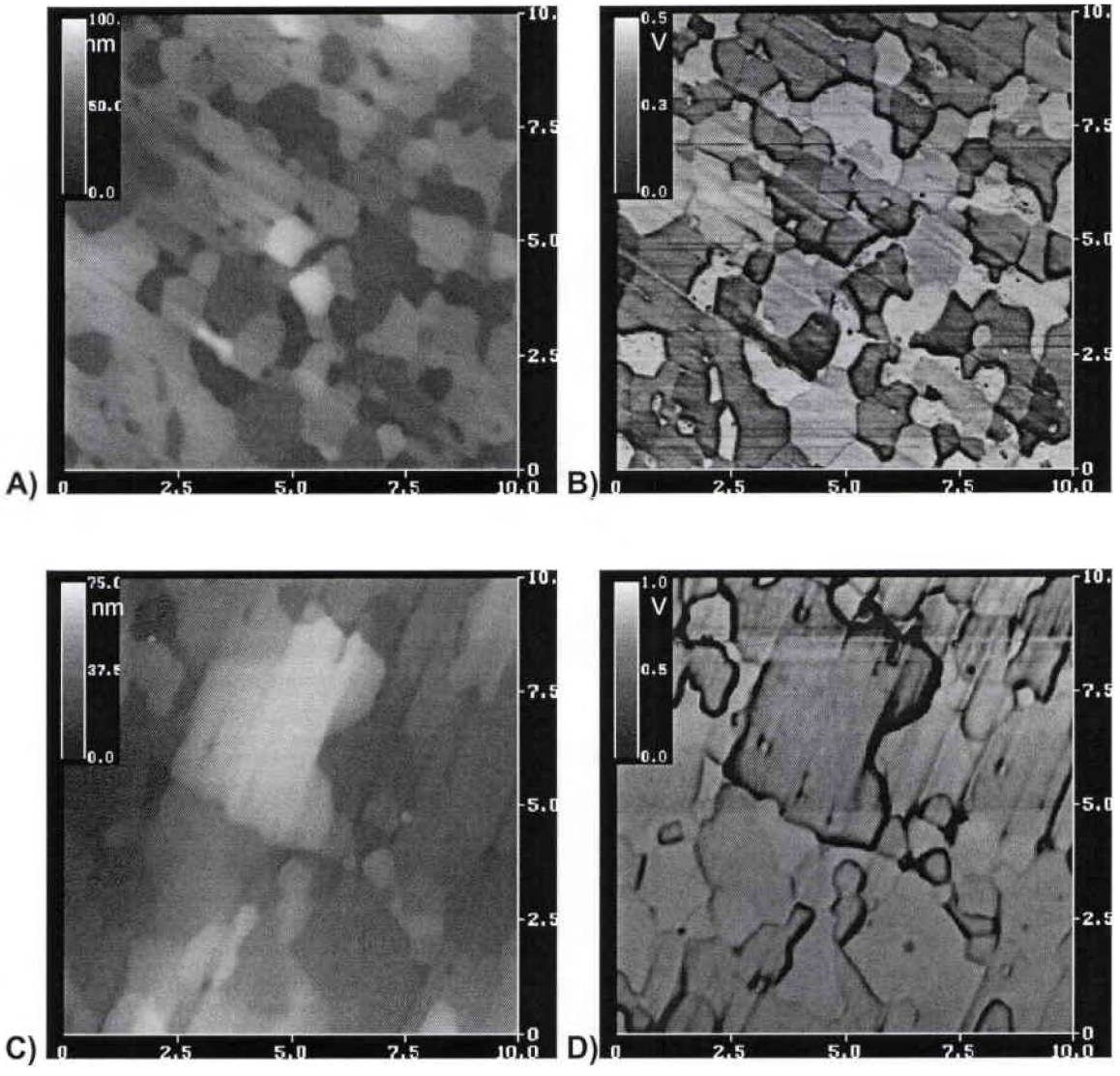

Figure 37: Comparison of Wafer Lots #1 & #5

A) Wafer #1 AFM Surface Topography Image, B) Wafer #1 UFM Amplitude Image, C) Wafer #5 AFM Surface Topography Image, D) Wafer #2 UFM Amplitude Image. Imaged area is 10 microns x 10 microns.

As observed on other materials the contrast in the UFM images was better than the AFM images. Though on these wafer samples, AFM images had a contrast level that compared favorably to that of the UFM image. The AFM images of the wafer surface are noticeably clearer than the AFM images in the earlier chapters. This is probably attributed to the hardness of the material and with the planing flat of the imaging surface during polishing. This resulted in sharp clear transition in the surface topography. The height changes are very defined steps with little smearing having occurred during polishing. A similar effect has been seen when the AFM's calibration sample, which has precision edges, when it has been imaged with the AFM-UFM method.

The images showed that although the polishing conditions and procedures were identical some of the samples had more surface scratches than the other samples. This indicates that there may be hardness difference in different regions of the sample. In the midst of the scratches both AFM and UFM produced images with reasonable contrast. The UFM images provided a better grain to grain contrast. A general examination of all of the UFM images showed that the grain shape as well as the grain size was different in each of the samples. The average grain sized varied from 1.0 to 1.8 μm.

An interesting feature is the differences in the shape of the grains. The sample lot #5 contains larger and elongated grains while sample lot #1 contains smaller and equiaxial grains. The two samples were processed under different conditions. One of the possible reasons for development of smaller as well as equiaxial grains can be attributed to the additives that interact chemically with

Al_2O_3-TiC. Bennison and Harmer (1983) have demonstrated the reduction of grain size and the development of equiaxial grains in Al_2O_3 due to the addition of MgO. Figure 38 taken from that reference is used to illustrate the effect of MgO addition.

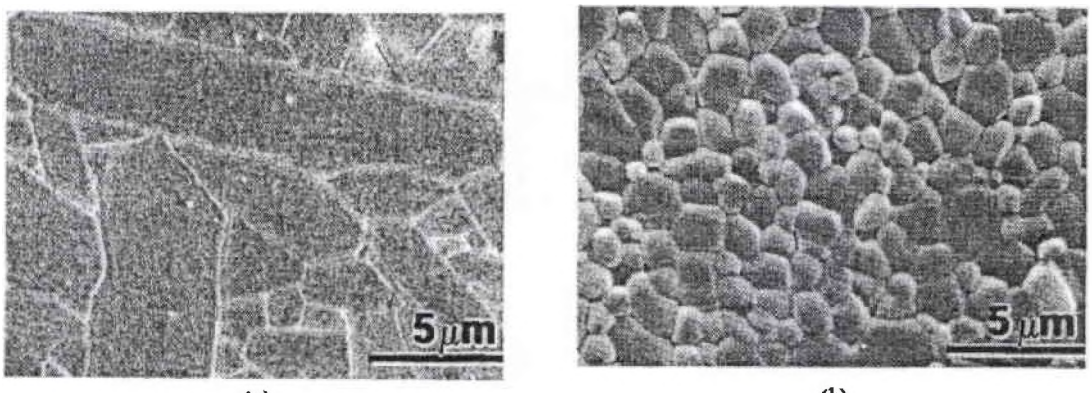

Figure 38: Effect of MgO Additive on Alumina
A) Dense, hot pressed alumina without MgO, B) with MgO addition
[Refer S.J. Bennison and M.P. Harmer, J. Am. Ceram. Soc., 66[5], C90-C92 (1983).]

This appears very similar to the effect seen in Figure 37. Without MgO addition in the hot pressing of alumina, large grains develop with tabular shape indicating a grain boundary anisotropy while in Figure 38b the MgO addition causes a more isotropic grain morphology [47]

One of the primary reasons for using UFM on the wafer samples was to gather information about the grain boundary region. Figure 39 shows a 3-D image of the various grain boundary responses from three different samples obtained at frequencies very close to one another. It should be noted that Figure 39A and 39B were inverted in order to make the boundary signal more

recognizable when viewing the printed image. Noticeable differences in the UFM response between the wafer lots in the grain boundary region can be observed.

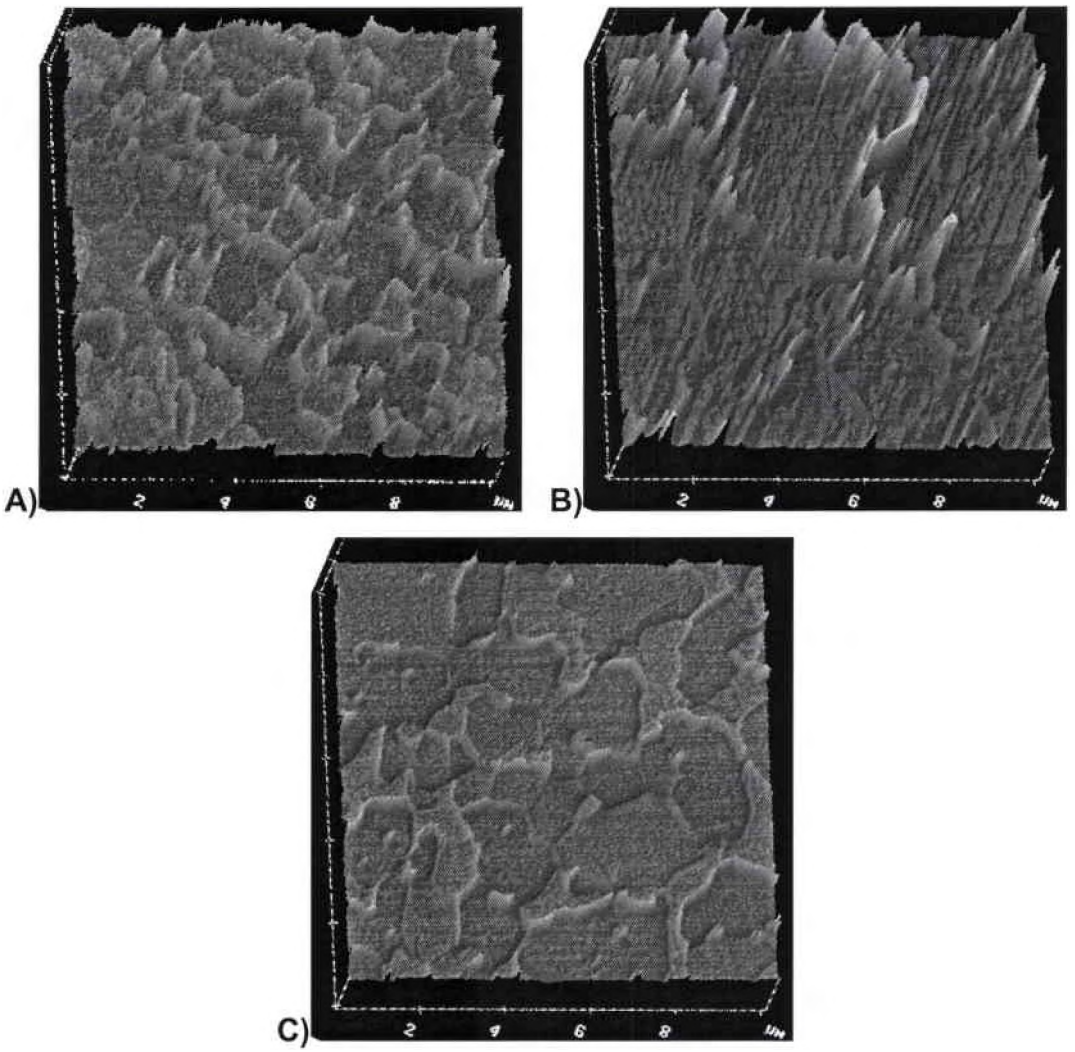

Figure 39: Comparison of Ultrasonic Response between 3 Wafer Lots A) Wafer #1 UFM Amplitude Image at 730 kHz, B) Wafer#5 UFM Amplitude Image at 730 kHz and C) Wafer #6 UFM Amplitude Image at 717 kHz. All images are 10 micron x 10 micron areas.

Although drawing firm conclusions utilizing the data presented is quite difficult, possible reasons for differences in the UFM response in the grain

boundary region will be presented. The grain boundary response of sample#1 is fairly uniform over the area of the image. It doesn't show large changes in around any of the grains. It should be noted that this material has equiaxial grains with a uniform distribution. The average grain size is smaller than the other samples. Sample lot #1 has the least grain pullout among the samples (private communications with end user).

The grain boundary response of sample #5 shows larger increases along certain grain boundaries. Closer examination reveals that the response on one side of the grain is dramatically different compared to the other side of the grain. This may indicate non-uniform binding between the grains and the boundary region. The grain pullout in the #5 samples were never directly compared to the sample lot #1 by the supplier. We believe that this non uniform response may be an indication of a higher likelihood for grain pullout.

Although the responses of the grain body and grain boundary region are very similar for sample #6, it has a higher grain pullout problem compared to sample #1. It seems that not only the boundary response but also the shape/size of the grains is important in reducing the grain pullout. This sample has elongated grains and a wider grain size distribution compared to sample #1

In the UFM images obtained at two different frequencies on the same region of the sample exhibited inversion of contrast for several grains. One such image is shown in Figure 40. The inversion of contrast has been attributed to the change in the interaction stiffness between the tip and the sample when the excitation frequency is changed over a resonant frequency. There is a cantilever-

sample system resonance in between the two frequencies chosen for imaging. Though contrast inversion can be used to highlight areas for image analysis, it makes difficult to conclude whether the stiffness of the material is high or low. Further investigation is required along these lines for obtaining more quantitative results.

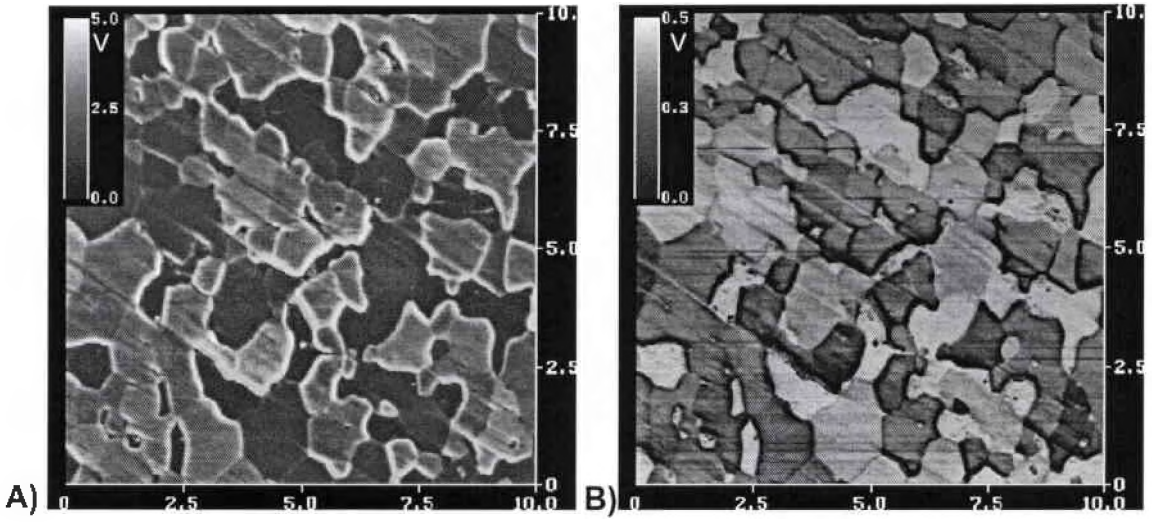

Figure 40: Contrast Inversion of Image on Wafer #1
A) UFM Amplitude Image at 430 kHz and B) UFM Amplitude Image at 730 kHz.

Contrast inversion is one of the reasons that the current technique is only qualitative. Judgements on the images can only state that there is a difference in the contact stiffness and determinations of which material is "hard" and which is "soft" can not be made. By changing the imaging frequency, one can get the hard material to look soft and vice a versa in the frequency range for our equipment. Additional information from other sources that elaborates on the material composition and location in the sample must be consulted before designations of which component is hard and which is soft are declared.

Comparison of Raw Wafer Material to the Same Material in a Finished Device

A comparison of the grain imaging of Al_2O_3-TiC wafer to actual Al_2O_3-TiCgrains in a microelectronic device has also been done. The AFM-UFM images on the raw substrate wafer material did closely match images acquired on the ABS rails of the slider, which is made from Al_2O_3-TiC. Figures 41 are images that were acquired of the Al_2O_3-TiC grain structure on the ABS surface from a head slider that was in use. Figure 41 was acquired at 835khZ.

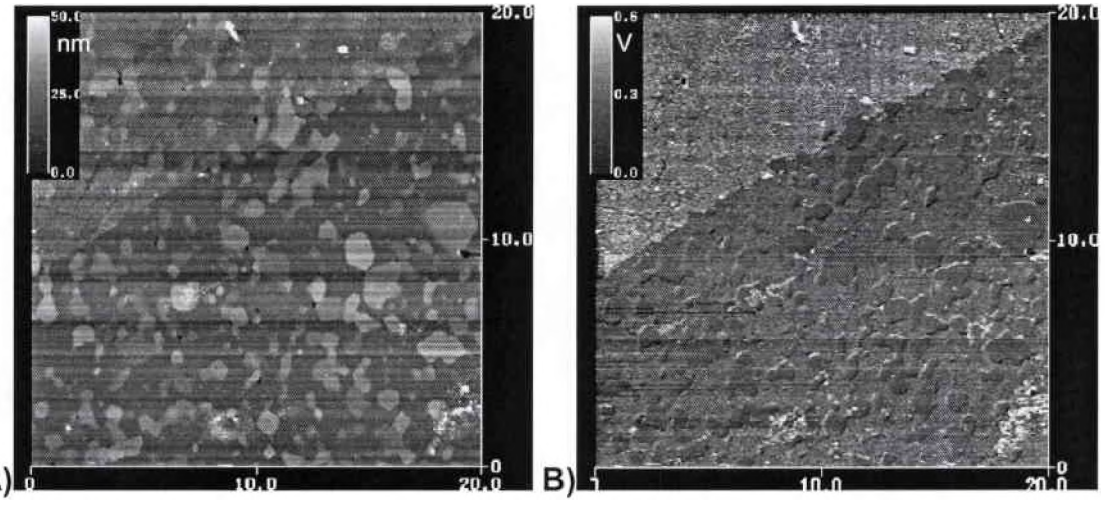

Figure 41: Al_2O_3-TiC Grain Structure in ABS Rails of a Head Slider
A) AFM Surface Topography Image B) UFM Amplitude Image
Imaged area is 20 microns x 20 microns

The grains are clearly visible in certain parts of the image while in some regions it appears as if there is a thin film on the surface. It is known that to improve wear and durability of the ABS surface on head sliders, a hard amorphous coating may be placed on the ABS surface [3]. The ABS rails may

also contact on a lubrication layer on the hard disc surface during shut down landings of the hard drive. So there are two possible causes for the film seen in the upper left half of Figure 41. Since the devices were cleaned ultrasonically in water and acetone, it is believed that the film is an applied wear coating and lubricant from the disc surface. Figure 42 and 43 are higher magnification images taken on the ABS surface of a device for comparison purposes. These images were acquired at different location on the ABS rails and show areas where remnants of the coating remain and areas where the coating is totally removed.

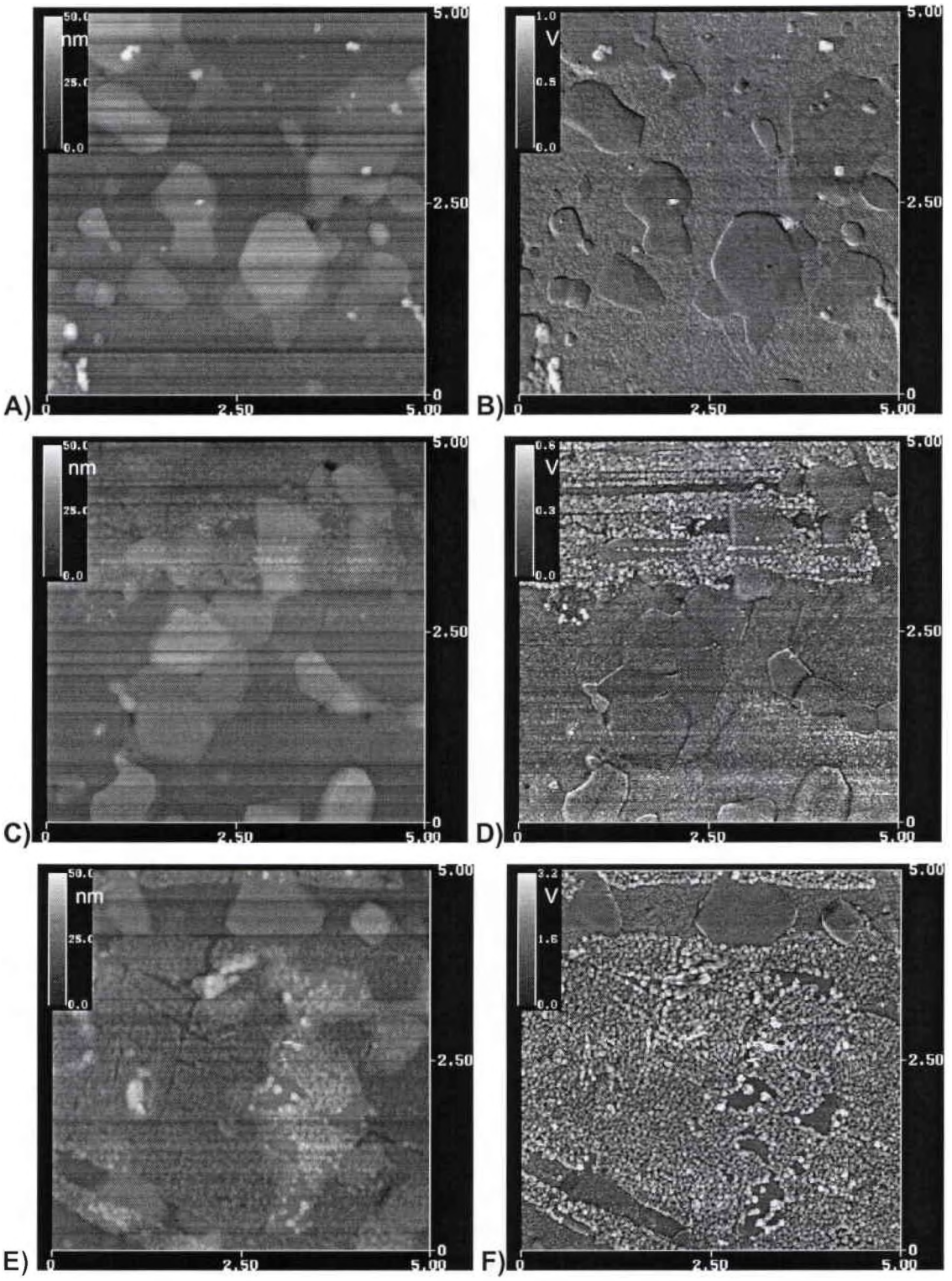

Figure 42: Higher Magnification Images of the ABS Rails

A, C & E are AFM topography images while B,D & F are the corresponding UFM Amplitude. All imaged area were 5 micron x 5 micron

Even higher magnification imaging shows an interesting feature on the ABS rails. It has not been determined if the specs (white) shown in Figure 43 are remnants of the coating or particulate in the material body itself.

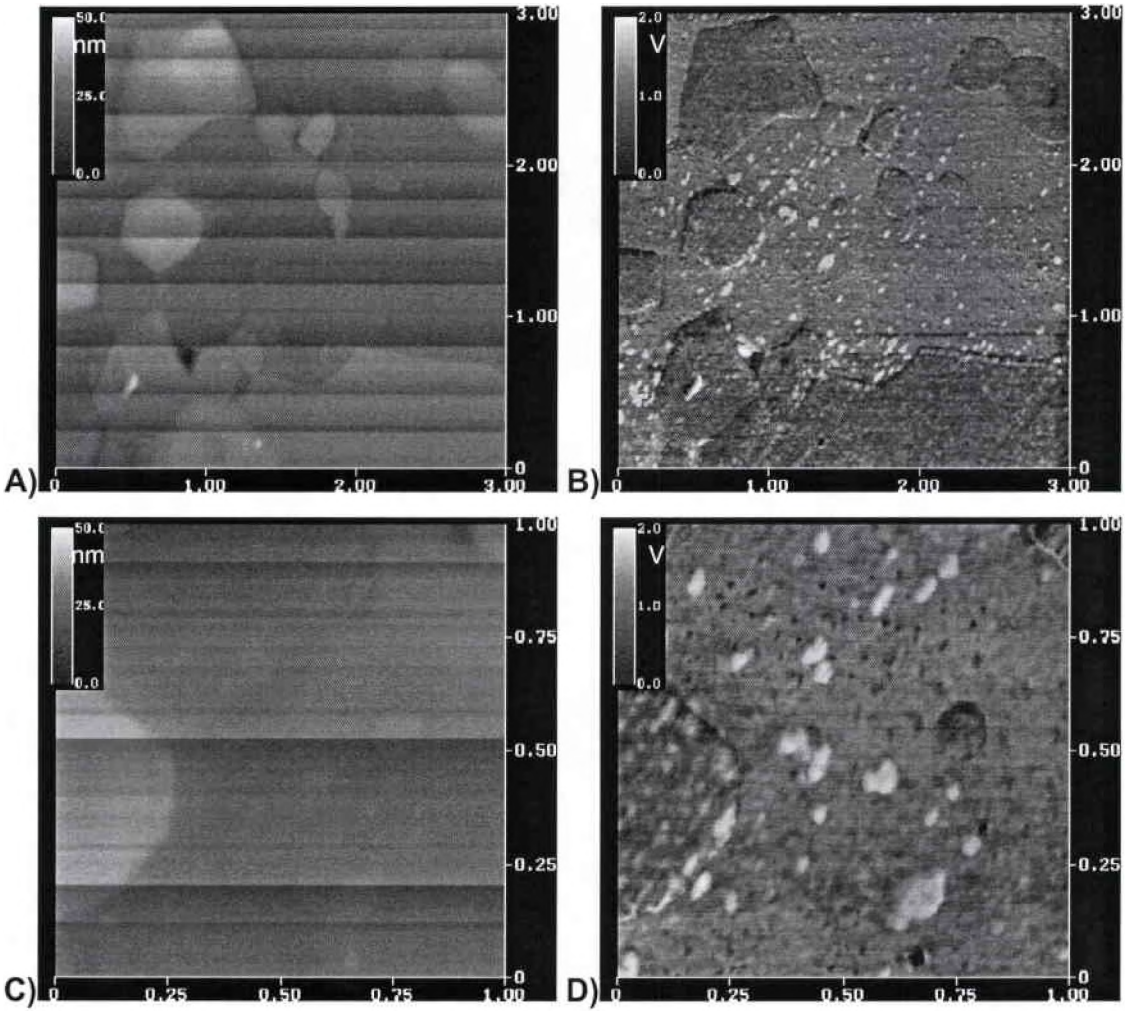

Figure 43: Further Higher Magnification Images of the ABS Rails. A & C are AFM topography images while B & D are the corresponding UFM Amplitude. All imaged area were 3 micron x 3 micron and 1 x 1 micron

It is believed that the difference in the response at the grain boundaries between different samples may be an indication of which samples may be more susceptible to grain pullout. It is also possible that the boundary response

difference could also have been caused by binders or alloying elements and thus is an indication of the location of these elements. These observations are qualitative in nature and need further careful investigation and additional manufacturing background information to be verified. Raw material wafer images appeared very similar to device imaging on a component made from the same material. It is believed that grains with an equiaxial nature are able to uniformly distribute stresses across their boundary regions making them more resistant to grain pullout. Further smaller equiaxial grain have less volume exposing their boundary region to a lower stress than larger equiaxial grains where the boundary region must hold a big section to the matrix.

Chapter 5

5.1) Summary

The AFM-UFM material characterization technique has been used to characterize materials and devices of importance in computer industry. The Al2O3-TiC ceramic matrix composite that is the base for the hard disc drive head sliders and the thin film copper wires of micron and sub micron width on the sliders have been characterized using AFM and UFM. In general, in all specimens examined, the contrast due to surface topography in the AFM images was weak and the majority of the characteristic features were submerged within the topography contrast. UFM images of the same region were found to have enhanced contrast and aided in visualizing the characteristic features.

The main difference between the two images is the origin of contrast. The contrast in AFM images is only due to surface height variations only. In the UFM, the tip interacts with the material underneath the scanning tip and senses the contact stiffness there by providing contrast due to the local Elastic variations in the material. Although the surface may be ultra smooth without topographical variations, the elastic modulus directly under the tip might vary from point to point and thus provide a means of enhanced contrast.

One of the applications carried out in detail is the investigation of laser surface treated head sliders whose main body is composed of Al2O3-TiC . Laser

treatment has been developed to adjust the surface crown of the head slider device by altering the top surface. Although the technique might have enormous advantages for modifying the miniaturized surface, this investigation showed formation defects generated by the heat shock on the surface in the laser treated regions.

Particularly, the UFM images showed the presence of micro and nano cracks on laser treated surfaces. Long cracks were observed to run along the grain boundary covering several grains. The microcracks appear to be running parallel to the laser line. Tiny (nano) cracks were observed to branch out from the main cracks. The UFM allowed for quicker and much easier location of cracks in the material than by conventional AFM imaging. Larger displacement around the stress free flanks of the crack enhances the visibility of the micro-cracks. The UFM images reveal the microstructural inhomogeneities and grain structure with a clear grain boundary contrast. Several grains were found to have separated from the matrix. Tiny spherical droplets with diameter in the range of 50 – 80 nm have been observed in only in laser treated region. UFM images clearly exhibit the presence of microcracks in the midst of the grain structure in the laser treated regions.

The development of the cracks have been explained based on the development of local thermal residual stress between Al2O3 grains due to thermal expansion difference between different crystallographic orientation. A crack running along the grain boundaries has been attributed to the difference in thermal expansion between Al2O3 and TiC. A large increase in the temperature

beyond the melting of the ceramic might be responsible for the formation of spherical droplets. All these features were observed only on the laser treated surface and were not observed in untreated surfaces.

Ultrasonic Force Microscopy imaging of copper microwires allowed for a detailed characterization of the grain structure. The microstructure of individual grains, voids, and other defects could be clearly imaged. Though contrast in UFM images could be attributed to elastic anisotropy, the images do not show grain to grain contrast inspite of copper being elastically anisotropic. It is well known for computer applications the copper microwires and interconnects should be produced with least amount of texture variations and advanced technique for growing only 1 preferred crystal direction are used.

Most often the wire grains in a microelectronic device will have very similar crystallographic orientations. Grains with similar crystallographic orientation have the same elastic modulus. This leads to lack of grain to grain contrast in UFM images of copper thin film wires. Although the grain to grain contrast is very small, the UFM images show large contrast at the grain boundaries. This dramatically helps in identifying the grains and performing grain structure analysis. The contrast at the grain boundary is intriguing and seems to originate from the atomic arrangements near the boundary of two grains. A plausible explanation for the increased contrast at the grain boundary in UFM image is attributed to the way the way the atoms are held together near the boundary. The enhanced contrast at the grain boundary has been utilized for quantitative determination of grain size in new as well as used devices. This has also helped

in identifying the defects, voids thought to be caused due to electron migration. The ability to monitor grain structure changes over time has many exciting applications in the development of a better understanding about the mechanisms that effect electromigration, grain size changes and device reliability on this nanometer scale.

Manufacturing of Al2O3 ceramic head sliders with no grain pullout or shedding of particles is very important for the integrity of the head sliders as well as hard disk. Since binding of the grain to the matrix trough the grain boundary region to the adjacent grains is the most important factor in grain pullout, the grain boundary response has been examined in different samples. Significant variations have been observed in the grain boundary response. Though qualitatively it is possible to attribute larger grain pullout to samples with unevenly distributed grain boundary response but it is difficult to draw sound conclusions with out further investigation.

In conclusion AFM-UFM combination has been utilized to investigate components of importance in the microelectronic industry. Defects in the micro and nanometer range generated due to laser treatment have been detected and examined in detail. Several interesting features have been observed and possible explanation has been provided. Grain structure on copper micro and nano wires has been investigated. The changes in grain structure due to service have been quantitatively determined. Defects, voids on copper wires due to use have been identifies and examined. The contrast at the grain boundary in copper as well as in Al2-O3 wafers has been examined in detail. The grain boundary

response in ceramic matrix has been found to vary significantly from region to region. This is a possible indication for larger grain pullout.

REFERENCES

1. Bhushan, B., "Handbook of Micro/ Nano Tribology:" CRC Series Mechanics and Material Science, CRC Press, New York, pp.7-80, 1995.

2. Binning, G., Quate, C.F., and Gerber C.H. "Atomic Force Microscope", *Physical review letters*, Vol. 56, No. 9, pp. 930-933, 1986.

3. Bhushan, B., "Tribology and Mechanics of Magnetic Storage Devices", Springer-Verlag, New York, 1990.

4. Maivald, P., Butt, H.J., Gould, SAC, Prater, C.B., Drake, B., Gurley, J.A., Elings, V.B. and Hansma, P.K., "Using force modulation to image surface elasticities with the atomic force microscope", *Nanotechnology*, Vol. 2, pp. 103-106, 1991.

5. Radmacher, M., Tillmann, R., Gaub, H.E., "Imaging Viscoelasticity by Force Modulation with the AFM," *Biophysical Society*, Vol. 65, 735-742, 1993.

6. Koinkar, V. and Bhushan, B., "Microtribological studies of Al_2O_3, Al_2O_3-TiC, polycrystalline and single crystal Mn-Zn ferrite", *Wear*, Vol. 202, pp. 110-122, 1996.

7. Zhou, L., Kato, K., Umehara, N., and Miyake, Y.," Friction and wear properties of hard coating materials on textured hard disk sliders", *Wear*, Vol. 243, pp. 133-139, 2000.

8. Yamanaka, K, "Ultrasonic Force Microscopy", *MRS Bulletin*, October 1996.

9. Burnham, N., Kulik, A.J., Gremaud, G., Gallo, P.J., and Oulevey, F. "Scanning local acceleration microscopy", *Journal of Vacuum Science and Technology*, Vol. 14, No. 2, pp. 794-799, 1995.

10. Rabe, U., and Arnold, W., "Acoustic Microscopy by atomic force microscopy", *Applied Physics Letters,* Vol. 64, No. 12, pp. 1493-1495, 1994.

11. Yamanaka, K. and Ogiso, H., "Ultrasonic Force Microscopy for nanometer resolution of subsurface imaging", *Applied Physics Letters*, Vol. 64, No. 2, pp. 178-180, 1994.

12. Yamanaka, K., Tsuji, T., Noguchi, Koike, T., and Mihara, T.,"Nanoscale elasticity measurement with in situ tip shape estimation in atomic force microscopy", *Review of Scientific Instruments*, Vol 71, No. 6, pp2403-2408, 2000.

13. Digital Instruments, "Dimensions™ 3000 Scanning Probe Microscope Instruction Manual", 1996.

14. Burnham, N., Kulik, A.J., Oulevey, F., Mayencourt, C., Gourdon, D., Dupas, E., Gremaud, G., "A Beginner's Guide to LPM Materials Properties Measurements", Micro/Nanotribology and its Applications edited by B. Bhushan, Kluwer Academic Publishers, pp.421-438, 1997.

15. Burnham, N., Gremaud, G., Kulik, A.J., Gallo, P.J., and Oulevey, F. "Materials properties measurements: choosing the optimal scanning probe microscope configuration", *Journal of Vacuum Science and Technology*, Vol. B-14, No. 2, pp. 1308-1312, 1996.

16. Burnham, N.A., Baker, S.P., Pollock, H.M., "Model for mechanical properties nanoprobes", *Journal of Materials Research*, Vol. No.9, pp. 2006-2014, 2000.

17. Rabe, U., Scherer, V., Hirsekorn, S., Arnold, W., "Nanomechanical surface characterization by atomic force acoustic microscopy", *Journal of Vacuum Science and Technology*, Vol. 15 #4, pp1506-1511, 1997

18. Chiu, A., Croll, I., Heim, D.E., Jones Jr., R.E., Kasiraj, P., Klaassen, K.B., Mee, C.D., Simmons, R.G., "Thin Film Inductive Heads", *IBM Journal of Research and Development*, Vol. 40, #3, pp. 283-300, 1996.

19. Menon, A. "Interface tribology for 100 Gb/In2", *Tribology International*, Vol. 33, pp. 299-308, 2000.

20. Tam, A.C., "Laser processes for precise microfabrication of magnetic disk drive components", *Riken Review*, Vol. 32, pp. 71-76, 2001.

21. Zhang, J.H., Lee T.C., Ai X., Lau, W.S." Investigation of the surface integrity of laser cut ceramics", *Journal of Materials Processing Technology*, Vol. 57, pp. 304-310, 1996.

22. Chen, G., Xu, X., Poon, C., Tam, A., "Laser Assisted microscale deformation of stainless steel and ceramics", *Optical Engineering*, Vol. 37, No. 10, pp. 2837-2842, 1998.

23. Gatzen, H., "Rigid disk slider micromachining challenges to meet microtribology needs", *Tribology International*, Vol. 33 pp. 337-342, 2000.

24. Fu, T.C., Suzuki, S., "Low stiction/low glide height-disk interface for high performance disk drives", *Journal of Applied Physics*, Vol. 85, No. 8, pp.5600-5605, 1999.

25. Liu J.J., Li W., Johnson K., "Current and Future approaches for laser texturing of thin film media", *IEEE Transactions on Magnetics*, Vol. 36, No. 1 pp. 125-131, 2000.

26. Lu Y.F., Song W.D., Hong M.H., " Laser removal of particles from magnetic head sliders", *Journal of Applied Physics,* Vol. 80, No. 1, pp. 499-504, 1996.

27. Zhou, L., Kato, K., Umehara, N., Miyake, Y., "Nanometre Scale island type texture with controllable height and area ratio formed by ion beam etching on hard disk head sliders", *Nanotechnology*, Vol. 10, pp. 363-372, 1999.

28. Smith, R.N., Surprenant, R.P., Kaminski, D.A.," Fracture Characteristics of an Aluminum Oxide Ceramic During Continuous Wave Carbon Dioxide Laser Cutting", *Proceeding ICALEO*, pp. 337-347, San Jose CA. 3-8 Nov 1991.

29. Poon, C. and Bhushan, B., "Nano-asperity contact analysis and surface optimization for magnetic head sliders/ disk contact", *Wear*, Vol. 202, pp. 83-98, 1996.

30. Gatzen, H., Ma, X., Scherge, M., Jhon, M.S., Bauer, C.L. "Observations regarding the tribological properties of SiC and ALTiC Sliders", *IEEE Transactions on Magnetics*, Vol. 32, No. 5, pp. 3783-3785, 1996.

31. Chekanov, A., Low, T., Alli, S., Liu, B., Teo, B.S., and Hu, S. "Microcracks of the Alumina of thin Film Head: Study and Simulation", *IEEE Transactions on Magnetics*, Vol. 31, No. 6, pp. 2991-2993, 1995.

32. Chekanov, A., Low, T., Alli, S.," Microcracks of the Thin Film Head Alumina: L and U cracks", *IEEE Transactions on Magnetics*, Vol. 32, No. 5, pp. 3696-3698, 1996.

33. Green, D. J. "An introduction to the mechanical properties of ceramics," Cambridge University Press, New York, 1998.

34. Ma, Q. "Fracture in Small Dimensions", Letter to the editor for 'Mechanical Properties in Small Dimensions Comments from Industry', *MRS Bulletin*, Vol. 27, #1, p52, 2002.

35. Singer, P. and Collin, G., "Copper CMP: a question of tradeoffs", *Semiconductor International*, Vol. 23, No.5, pp73-84, 2000.

36. McClusker, N.D., Gamble, H.S., Armstrong, B.M., "Surface Electromigration in copper interconnects", *Microelectronics Reliability*, Vol. 40, pp. 69-76, 2000.

37. Toh, B.H.W., McClusker, N.D., McNeill, D.W., Gamble, H.S. and Len V., "Surface Electromigration of sputtered copper patterned using ion milling or chemical mechanical polishing", *Journal of Materials Science: Materials in Electronics*, Vol. 12, pp. 307-312, 2001.

38. Hasegawa, M., Hirai, Y., "Microscopic observation of Cu damascene interconnects grains using x-ray microbeam", *Journal of Applied Physics*, Vol. 90, No. 6, PP 2792-2795, 2001.

39. Tsui, T. "The Industrial Significance of Understanding Dislocation Behavior in Thin Films, Letter to the editor for 'Mechanical Properties in Small Dimensions Comments from Industry', *MRS Bulletin*, Vol. 27, #1, p53, 2002

40. Jiang, Q.T., Nowell, M., Foran, B., Frank, A., Havemann, R.H., Parihar,V., Augur, R.A., and Luttmer, J.D., "Analysis of Copper Grains in Damascene Trenches after Rapid Thermal Processing or Furance Anneals", *Journal of Electronic Materials*, Vol. 31, No. 1, pp. 1015, 2002.

41. Besser, P.R., Zschech, E., Blum, W., Winter, D., Ortega, R., Rose, S., Herrick, M., Gall, M., Thrasher, S., Tiner, M., Baker, B., Braeckelman, G., Zhao, L., Simpson, C., Capasso, C., Kawasaki, H., Weitzman, E., " Microstructural Characterization of Inlaid Copper Interconnect Lines", *Journal of Electronic Materials*, Vol. 30, No. 4, pp.320-330, 2001.

42. Schumaker, E. J., Shen, L., Ruddell, M. J., Sathish, S., Murray, P. T., "Ultrasonic force microscopic characterization of nanosized copper particles", *Nanophase and Nanocomposite Materials III. Symposium (Materials Research Society Proceedings Vol. 581),* pp. 473-477, 2000.

43. Hau-Riege, C.S., Thompson, C.V., "Use of scanned laser annealing to control the bamboo grain length of Cu Interconnects", *Applied Physic Letters*, Vol.77, No. 3, 2000.

44. Truell, R., Elbaum, C., Chick, B., "Ultrasonic Methods in Solid State Physics", Academic Press, New York, pp.370, 1969.

45. Sathish, S., Fossheim, K., Bye, T., "Imaging of Grain Structure of Copper by Scanning Acoustic Microscopy", *Journal of Material Science Letters*, Vol. **7**, No 7, p735-737, 1988.

46. 3M Advanced Ceramic Program, "3M ME4000 Aluminum Oxide-Titanium Carbide Ceramic Brochure", copyright 3M, 1999.

47. Chiang, Y.M., Birnie III, D., Kingery, W.D., "Physical Ceramics: Principles for Ceramics Science and Engineering", John Wiley & Sons, Inc. pp. 351-500, 1997.